SAFETY ASSESSMENT OF R/C COLUMNS AGAINST
EXPLOSIVE ATTACKS BY VEHICLE OR HUMAN FROM EXTERIOR

A THESIS SUBMITTED TO
THE GRADUATE SCHOOL OF NATURAL AND APPLIED SCIENCES
OF
MIDDLE EAST TECHNICAL UNIVERSITY

BY

KARTAL ALTUNLU

IN PARTIAL FULFILLMENT OF THE REQUIREMENTS
FOR
THE DEGREE OF MASTER OF SCIENCE
IN
CIVIL ENGINEERING

FEBRUARY 2008

Approval of the Thesis;

SAFETY ASSESSMENT OF R/C COLUMNS AGAINST EXPLOSIVE ATTACKS BY VEHICLE OR HUMAN FROM EXTERIOR

Submitted by **KARTAL ALTUNLU** in partial fulfillment of the requirements for the degree of **Master of Science in Civil Engineering Department, Middle East Technical University** by,

Prof. Dr. Canan Özgen
Dean, Graduate School of **Natural and Applied Sciences**   _____

Prof. Dr. Güney Özcebe
Head of Department, **Civil Engineering**   _____

Assist. Prof. Dr. Ahmet Türer
Supervisor, **Civil Engineering Dept., METU**   _____

Examining Committee Members:

Assoc. Prof. Dr. Can Balkaya
Civil Engineering Dept., METU   _____

Assist. Prof. Dr. Ahmet Türer
Civil Engineering Dept., METU   _____

Assoc. Prof. Dr. İ.Özgür Yaman
Civil Engineering Dept., METU   _____

Assist. Prof. Dr. Alp Caner
Civil Engineering Dept., METU   _____

Ateeq Ahmad (M.Sc)
General Manager, Proya Software & Trade Inc.   _____

Date: _____

I hereby declare that all information in this document has been obtained and presented in accordance with academic rules and ethical conduct. I also declare that, as required by these rules and conduct, I have fully cited and referenced all material and results that are not original to this work.

Name, Last name: Kartal Altunlu

Signature   :

ABSTRACT

SAFETY ASSESSMENT OF R/C COLUMNS
AGAINST EXPLOSIVE ATTACKS BY VEHICLE OR HUMAN FROM
EXTERIOR

Altunlu, Kartal

M.S., Department of Civil Engineering

Supervisor : Assist. Prof. Dr. Ahmet Türer

Reinforced concrete structures may be subjected to blast loads together with static loads during their service life. Important buildings may be attacked by using explosives as a part of increasing global terrorist activities. Evaluation of blast phenomena for economically and strategically significant buildings is especially important, in order to analyze and design their structural members subjected to air blast loading. Understanding nature of explosions, which are loading characteristics and relation to selected parameters such as explosive type, quantity, and distance, were studied in this thesis. Earlier studies found in the literature survey on explosives, blast, and behavior of structural elements were investigated. Behavior of structures under blast load was described in terms of pressure magnitude, distribution, and reflection phenomena. Simple design, assessment guidelines, and useful charts were developed. A computer program was generated using MATLAB programming language, which automatically generates the air blast pressure versus time data resulting from an air explosion in addition to finite element model formation and dynamic time stepping analysis of a reinforced concrete column. The shear and moment capacities can be calculated and compared against dynamically calculated

demand under known axial column force; therefore, vulnerability of a column under blast loading is evaluated. The results of the numerical analyses indicated that failure mechanism of columns is mostly shear failure instead of moment (i.e., plastic hinge and mechanism formation).

Keywords: Explosive, Blast, Terrorist, Safety, Reinforced concrete column.

ÖZ

BETONARME KOLONLARIN YÜKLÜ ARAÇ VEYA İNSANLA
DIŞARIDAN PATLATMALI TERÖRİST SALDIRILARA KARŞI
EMNİYETİNİN BELİRLENMESİ

Altunlu, Kartal

Yüksek Lisans, İnşaat Mühendisliği Bölümü

Tez Yöneticisi : Yrd. Doç. Dr. Ahmet Türer

Şubat 2008, 85 sayfa

Betonarme yapılar, hizmet süreleri sırasında statik yüklere ek olarak patlama yüklerine de maruz kalabilirler. Önemli yapılar, artan terörist eylemler sebebiyle patlayıcıların kullanıldığı saldırılara hedef olabilirler. Patlama olgusunu değerlendirmek, ekonomik ve stratejik önem taşıyan yapıları patlama yükleri altında analiz ve dizayn etmek açısından önem taşımaktadır. Bu tezde, patlamanın doğası, yükleme karakteristikleri, tipi, miktarı ve uzaklığı gibi parametrelerle ilişkilendirilerek incelenmiştir. Patlayıcılar, patlatma olgusu ve açığa çıkan yükler altında yapısal elemanların davranışı hakkında geçmişte yapılmış çalışmalar incelenmiştir. Patlama yükü etkisindeki elemanların davranışı, basınç büyüklüğü, dağılımı ve yansıma olgusu altında incelenmiştir. Basitleştirilmiş dizayn ve değerlendirme kriterleri geliştirilmiştir. Kullanışlı abaklar hazırlanmıştır. MATLAB programlama dili kullanılarak bir analiz programı yazılmıştır. Program, patlama basıncı – zaman ilişkisini oluşturur ve betonarme bir kolonun bu yükler altındaki davranışını dinamik olarak sonlu elemanlar yöntemiyle analiz eder. Kesme ve moment kapasiteleri hesaplanır ve dinamik yöntemle elde edilen yüklerle karşılaştırılır. Böylece kolonun yaralanabilirliği değerlendirilmiş olur. Programdan elde edilen sonuçlar

kolonun kırılma mekanizmasının çoğunlukla moment yerine kesme olduğunu göstermiştir.

Anahtar Kelimeler: Patlayıcı, Patlama, Terörist, Güvenlik, Betonarme kolon.

To My Parents

ACKNOWLEDGMENTS

TABLE OF CONTENTS

LIST OF FIGURES

FIGURES

LIST OF TABLES

TABLES

LIST OF SYMBOLS

a	Acceleration
A_c	Area of column section
A_s	Area of reinforcing steel
b_w	Width of column
d	Depth of column
D	Apparent crater diameter
D_r	Actual crater diameter
E	Modulus of elasticity
f_{ck}	Characteristic compression strength of concrete
f_{ctd}	Characteristic tension design strength of concrete
f_{yk}	Characteristic yield strength of reinforcing steel
H_c	Height of burst
H_2	Apparent depth of the crater
H_{EXP}^{d}	Heat of detonation of explosive in question
H_{TNT}^{d}	Heat of detonation of TNT
i	The total equivalent triangular pulse
i_{ra}	Reflected impulse
I	Moment of inertia
K	Curvature
L	Length of column
m	Mass
M_p	Plastic moment capacity
N_d	Axial force of column
P_{so}	Peak positive incident pressure
$P_{so}-$	Peak negative incident pressure
P_{ra}	Peak reflected pressure
P_s-	Amplitude of the negative phase

p_o	Ambient atmospheric pressure
p_o	Ambient air pressure
p_s	Peak static air pressure
q_o	Peak dynamic pressure
q_s	Maximum dynamic pressure
R	Distance from charge centre
R_c	Radius of a spherical charge of condensed high explosive
R_d	Radius of detonation of wavefront
R_G	Actual ground distance
s	Space between stirrups
t_A	The shock front arrives at a given location at time
t_0	Positive phase duration
t_o-	Negative phase duration
t_{of}^-	Fictitious duration
U	Shock front velocity
U_s	Blast wavefront velocity
V_n	Nominal shear strength of R/C section
V_s	Nominal shear strength provided by shear reinforcement
V_c	Nominal shear strength provided by concrete
W	Charge mass in TNT equivalence
W_E	Effective charge weight
W_{EXP}	Weight of the explosive in question
W_M	Distributed load
Z	Scaled distance
ρ_o	Density of air
δ	Displacement
α	Angle of incidence

CHAPTER 1

INTRODUCTION

International economic pressures and unbalance of power caused by globalization leads to increased number of terrorist activities, which primarily targets civil infrastructure such as strategically important buildings and bridges. Similarly, gas stations located close to residential buildings sometimes may explode due to lack of control and ignorance. Resistance of structures against wind, snow, and earthquakes are commonly studied by civil engineers. However, existing codes and regulations often fail to set the standards for blast loading calculation methods and related safety evaluation. Only technical manuals for military structures include such design parameters.

Attacking strategically important buildings is not a new issue but events occurred during the last decades show the importance of this topic. Especially attacks using ammonium nitrate or TNT loaded vehicles can easily reach to the facade of buildings and can cause extensive damage to the exterior columns and beams. Buildings can collapse partially or totally as a result of blast loading as one or multiple columns fail. The beam-column joints no longer being supported by columns not only increase their span length to almost double the original span length, but also the tension reinforcement location at the joints being top of the beam would cause a great weakness for bending of the unsupported large span. Including the dynamic effect of immediate removal of a column, it is easy to expect that the supported columns, beams, and slabs above the collapsed column will fail by its own weight.

In this thesis, out-of-plane loading caused by exterior explosions and related effects on the columns were investigated and explained. Explosive types,

samples of real-life bomb attacks, structural behavior, and related calculations are given in the following chapters.

1.1 OBJECTIVES

Within the objective of this study, it is intended to;

- Expand knowledge about blast loads and structural response:
    - Evaluate the blast phenomena (air, surface, confined, pressure-distance-time relationships, crater size, etc…),
    - Investigate and understand behavior of structures under blast loading.
- Develop an analysis program in MATLAB for time-history analysis of R/C columns (10 nodes, 9 members, central difference method)
- Understand the behavior of R/C columns subjected to air blast loading and generate simplified empirical relationships.

1.2 SCOPE

The scope of this study is,

- To research the literature on:
    - Extreme loadings
    - Explosives types & blast wavefront parameters
    - Blast loading on structures, international codes,
    - Global cases etc.
- To write a computer program on dynamic response of R/C columns subjected to blast loading
- To list general assumptions, generate flow chart, define analytical model
- To conduct sample problems
- To find empirical relationships to evaluate columns for blast loading (define a simplified method)

- To investigate most common strengthening methods against blast loading.
- To draw conclusions

CHAPTER 2

LITERATURE SURVEY / BACKGROUND

2.1 EXPLOSIVES

2.1.1 Defining an Explosion

An explosion defined as a large-scale, rapid and sudden release of energy. Explosions can be categorized as physical, nuclear or chemical events.

In physical explosions, energy may be released from the catastrophic failure of a cylinder of compressed gas, volcanic eruptions or even mixing of two liquids at different temperatures.

In nuclear explosions, energy is released from the formation of different atomic nuclei by the redistribution of the protons and neutrons within the interacting nuclei.

Chemical explosions involve the rapid oxidation of fuel elements (carbon and hydrogen atoms) contained within the explosive compound.

Combustion is the term used to describe any oxidation reaction, including those requiring the presence of oxygen from outside as well as those that use oxygen as an integral part of the reacting compound. When applied to particular case of the oxidation of gun propellants, the process is usually detonated as burning [2]. There are two combustion processes known as;

- *Deflagration* process, where explosive materials can decompose at a rate much below the speed of sound in the material.

- *Detonation* produces a high intensity shock wave. The reaction is accompanied by large pressure and temperature gradients at shock wave front and the reaction is initiated instantaneously.

2.1.2 Types of Bombs and Properties

Explosive materials are classified considering their physical state: solids, liquids, or gases. Although flammable chemicals and propellants may be classified as potentially explosive materials, solid explosives are primarily high explosives. Liquid and gaseous explosives include a wide variety of materials used in the manufacture of chemicals, fuels, and propellants. The blast pressure environment produced will differ for a particular material. Because procedures used in manufacturing, storage, handling, physical and chemical characteristics, may differ the blast effects of an explosive material.

The blast effects of solid materials are best known. The blast pressures, impulses, durations, and other blast effects of an explosion have been well established. Unlike high-explosive materials, other solid, liquid, and gaseous explosive materials have differences of their blast pressure output. In many cases only a portion of the total mass of the explosive (effective charge weight) is involved in the detonation process. The remainder of the mass is usually consumed by deflagration. Material's chemical energy is dissipated as thermal energy which may cause fires or thermal radiation damage in deflagration process. TNT and ammonium nitrate are most commonly used explosives.

TNT: Perhaps the most widely known explosive compound in TNT, a member of the nitro-explosive class which contains the $-NO_2$ group linked to a carbon atom, which was developed by the German Wilbrand in 1863. The full name is

2,4,6-trinitrotoluene of gross formula $C_7H_5O_6N_3$ which is made by the action of nitric and sulphuric acids on toluene (methyl benzene). It exists as a pale yellow-brown crystalline solid with a melting point of $80.6^{\circ}C$, a mass specific energy of 4520 kJ/kg and produces 0.73 m^3 of gas per kilo-gramme. TNT is used as filling for military munitions where it is usually mixed with other explosives such as RDX, HMX or ammonium nitrate. As well as being a very effective explosive, TNT is widely accepted as the basis for comparison with other condensed high explosive materials. [2]

Ammonium Nitrate (NH_4NO_3): It is used as manure and obtainable relatively. However Ammonium Nitrate is not used as an explosive but as a mixture. Common property of mixtures are that ANFO (Ammonium Nitrate + Fuel Oil) and AMATOL (Ammonium Nitrate + Tri Nitro Toluene). Their detonation speeds are between 2000 and 5000 m/s. Pulverizing and mixing with acceptable fuel make the material explosive. In order to produce an explosive, ammonium nitrate should be contributed in appropriate rate of fuel, be in covered medium (steel container) and ignited with a primary explosive (dynamite or hand grenade). In this way, detonation speed can be increased to 6000 m/s.

In the terrorist attacks, improvised explosive devices are commonly used. An improvised explosive device can be almost anything with any type of material and initiator. It is a "homemade" device that is designed to cause death or injury by using explosives alone or in combination with toxic chemicals, biological toxins, or radiological material. Improvised explosive devices can be produced in varying sizes, functioning methods, containers, and delivery methods. Improvised explosive devices can utilize commercial or military explosives, homemade explosives, or military ordnance and ordnance components. They are unique in nature because the improvised explosive device builder has had to improvise with the materials at hand. Designed to defeat a specific target or type of target, they generally become more difficult

to detect and protect against as they become more sophisticated [11]. Improvised explosive devices fall into three types of categories which are Package Type, Vehicle-Borne and Suicide Bomb. Explosive standards of vehicle bombs are shown in Table 2.1. Larger vehicles enable larger amounts of explosive that can be used, resulting in a greater effect. Functioning of devices can vary within the same methods as the package types and can have the same common characteristics or indicators as other improvised explosive devices.

Table 2.1 BATF (Bureau of Alcohol Tobacco and Firearms) Explosive Standards [11]

ATF	Vehicle Description	Maximum Explosives Capacity	Lethal Air Blast Range	Minimum Evacuation Distance	Falling Glass Hazard
	Compact Sedan	500 pounds 227 Kilos (In Trunk)	100 Feet 30 Meters	1,500 Feet 457 Meters	1,250 Feet 381 Meters
	Full Size Sedan	1,000 Pounds 455 Kilos (In Trunk)	125 Feet 38 Meters	1,750 Feet 534 Meters	1,750 Feet 534 Meters
	Passenger Van or Cargo Van	4,000 Pounds 1,818 Kilos	200 Feet 61 Meters	2,750 Feet 838 Meters	2,750 Feet 838 Meters
	Small Box Van (14 Ft. box)	10,000 Pounds 4,545 Kilos	300 Feet 91 Meters	3,750 Feet 1,143 Meters	3,750 Feet 1,143 Meters
	Box Van or Water/Fuel Truck	30,000 Pounds 13,636 Kilos	450 Feet 137 Meters	6,500 Feet 1,982 Meters	6,500 Feet 1,982 Meters
	Semi-Trailer	60,000 Pounds 27,273 Kilos	600 Feet 183 Meters	7,000 Feet 2,134 Meters	7,000 Feet 2,134 Meters

2.2 BLAST WAVES AND BLAST LOADING

As has been described, explosions liberate large amounts of energy which produces very high local pressures. This pressure disturbance moves outwards

develops into a blast wave. In the following sections blast waves produced by the detonation of high explosive materials in free air and on the ground are discussed with particular reference to conditions at the blast wavefront.

2.2.1 Spherical Charges of Condensed High Explosive

Formation, description and effects of blast are analyzed in three locations. The first location is where the detonation of explosive materials occurs. The second is the region outside the charge where the blast wave is formed. Third is the region where the blast wave generates the structural loading.

2.2.1.1 Inside The Charge

A spherical charge of condensed high explosive of radius R_c is considered as shown in Figure 2.1. Detonation wavefront is at radius R_d. The reaction zone is in thin region.

In zone A, pressure, density, particle velocity and temperature are all varying with radius from charge centre. In zone B, beyond the detonation wave front of radius R_d, the unreacted explosive is at ambient pressure. Zone C is at surrounding atmospheric conditions and the air has specific energy and sound velocity.

2.2.1.2 Outside the Charge

A plane wave front is shown in Figure 2.2. In zone I is the region of expanding gases. In zone II is the region of the surrounding compressed air.
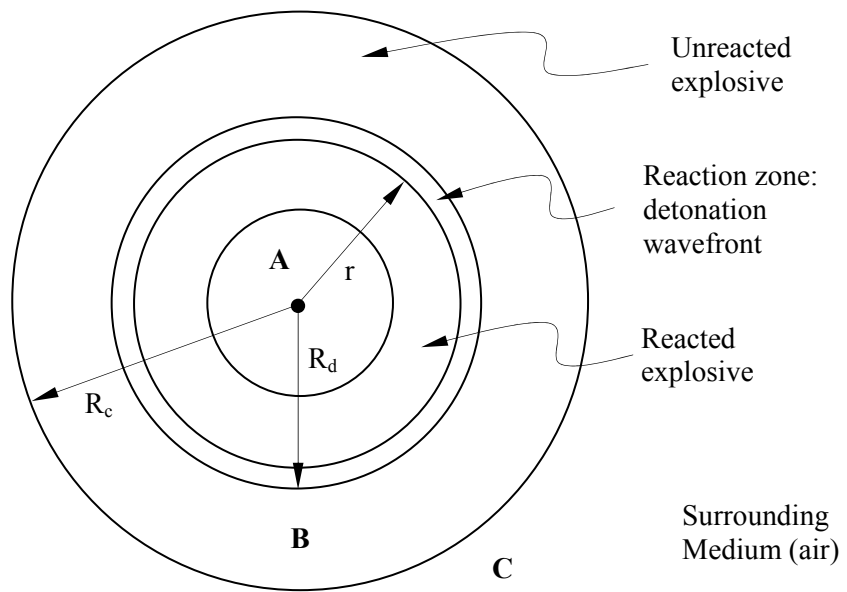
Figure 2.1 Inside the charge [2]
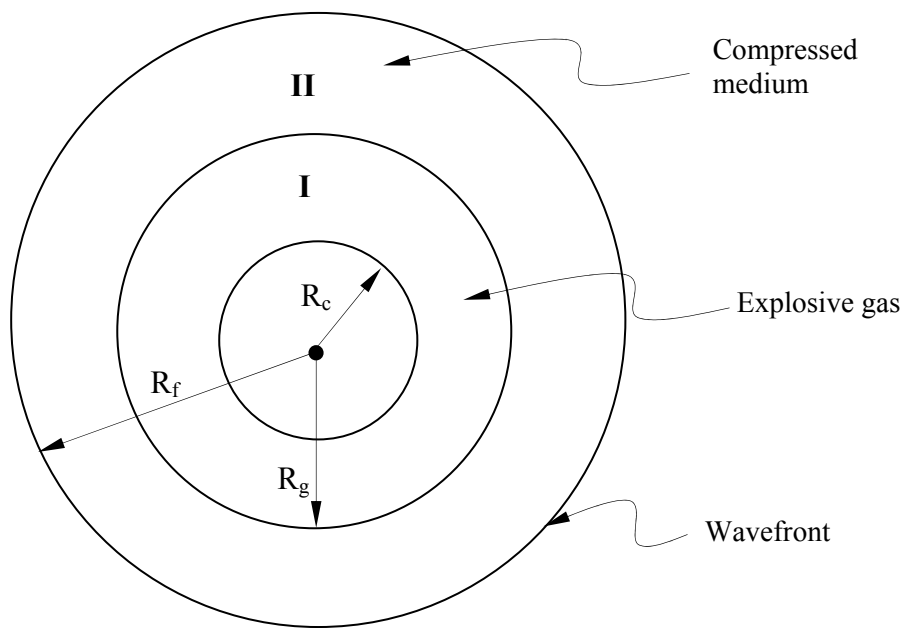
Figure 2.2 Outside the charge [2]

2.2.2 Blast Wavefront Parameters

There are several overpressure equations developed for blast wavefront parameters. Firstly Rankine and Hugoniot in 1870 presented to describe normal shocks in ideal gases.

$$U_s = \sqrt{\frac{6p_s + 7p_o}{7p_o}} a_o \tag{1}$$

$$\rho_s = \frac{6p_s + 7p_o}{p_s + 7p_o} \rho_o \tag{2}$$

$$q_s = \frac{5p_s^2}{2(p_s + 7p_o)} \tag{3}$$

U_s =Blast wavefront velocity

p_o =Ambient air pressure

p_s =Peak static air pressure

ρ_o =Density of air

q_s =Maximum Dynamic pressure

The second equation was developed by Brode in 1950's. Brode's equations lead to results for near field (pressure is over 10 bar) and medium to far field (pressure is between 0.1 and 10 bar).

$$p_s = \frac{6.7}{Z^3} + 1 \ bar \ (for \ p_s > 10 \ bar) \tag{4}$$

$$p_s = \frac{0.975}{Z} + \frac{1.455}{Z^2} + \frac{5.85}{Z^3} - 0.019 \ bar \ (for \ 0.1 < p_s < 10 \ bar) \tag{5}$$

Z is scaled distance given by,

$$Z = \frac{R}{W^{1/3}} \tag{6}$$

R is the distance from charge centre and W is the charge mass in TNT equivalence. The equations presented by Henrych are similar form to those of Brode (Figure 2.3).

$$p_s = \frac{14.072}{Z} + \frac{5.54}{Z^2} - \frac{0.357}{Z^3} + \frac{0.00625}{Z^4} \ bar \ (0.05 \le Z < 0.3) \qquad (7)$$

$$p_s = \frac{6.194}{Z} - \frac{0.326}{Z^2} + \frac{2.132}{Z^3} \ bar \ (0.3 \le Z \le 1) \qquad (8)$$

$$p_s = \frac{0.662}{Z} + \frac{4.05}{Z^2} + \frac{3.288}{Z^3} \ bar \ (1 \le Z \le 10) \qquad (9)$$
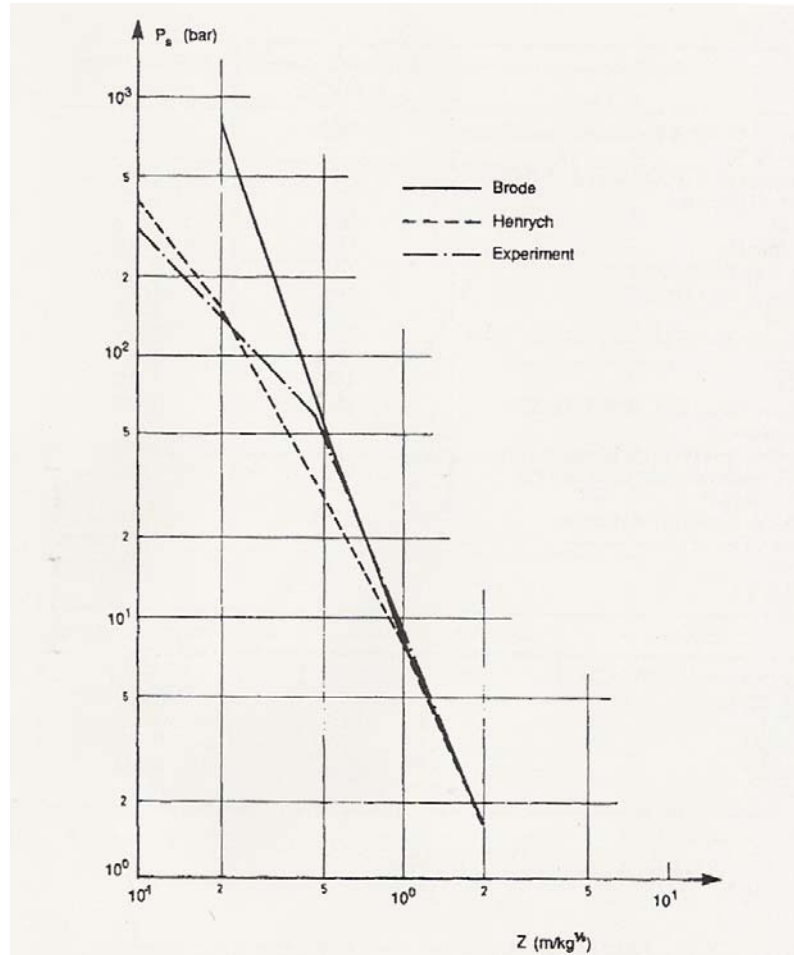
Figure 2.3 Side-on peak overpressure vs. scaled distance: comparisons between experiment and analysis [2]

2.2.3 TNT Equivalency

The main parameter of blast effects is connected to output of bare spherical TNT explosive. Other potentially mass-detonating materials are included by

11

relating the explosive energy of the "effective charge weight" of those materials to that of an equivalent weight of TNT. The material shape (flat, square, round, etc.), the number of explosive items, explosive confinement (casing, containers, etc.), and the pressure range being considered (close-in, intermediate or far ranges) may affect the equivalency of material compared to TNT. The effects of the energy output on explosive material relative to that of TNT, can be expressed as function of the heat of detonation of the various materials. Where

$$W_E = \frac{H_{EXP}^d}{H_{TNT}^d} W_{EXP} \tag{10}$$

W_E=effective charge weight

W_{EXP}=weight of the explosive in question

H_{EXP}^d=heat of detonation of explosive in question

H_{TNT}^d=heat of detonation of TNT

TNT is the reference explosive and quantifying blast waves from sources other than TNT is the first stage which is to convert the actual mass of the charge into a TNT equivalent mass. Some TNT equivalence factors for range of explosives are shown in Table 2.2.

Table 2.2 TNT Equivalence [2]

Explosive	TNT Equivalence Factor
Amatol 80/20 (80% ammonium nitrate, 20% TNT)	0.586
C-4 (91% RDX, 9% plasticizer)	1.27
Compound B (60% RDX, 40% TNT)	1.148
RDX (Cyclonite)	1.185
HMX	1.256
Mercury fulminate	0.395
Nitroglycerin (liquid)	1.481
PETN	1.282
Pentolite 50/50 (50% PETN, 50% TNT)	1.129
TNT	1.000
Torpex (42% RDX, 40% TNT, 18% Aluminum)	1.667

2.2.4   Blastwave Pressure-Time History

The explosive material is converted into a very high pressure gas at very high temperatures by release of energy from detonation. A pressure is very strong shock wave supported by hot gases and propagates radially into the surrounding atmosphere. The shock front, termed the blast wave, is characterized by an almost instantaneous rise from ambient pressure to a peak incident pressure P_{so} (Figure 2.4).
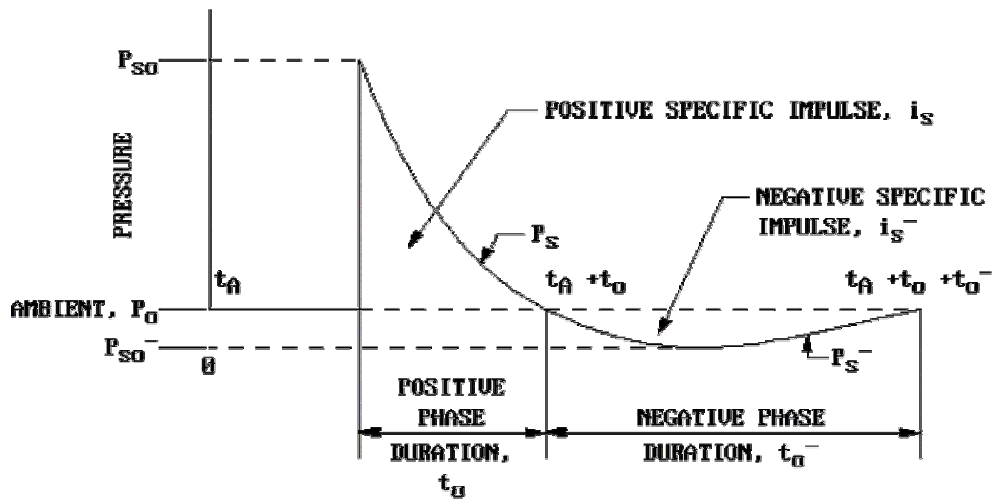
Figure 2.4 Free-field pressure-time variation [3]

At any point away from the burst, the pressure disturbance has the shape shown in Figure 2.4. The shock front arrives at a given location at time t_A and, after the rise to the peak value, P_{so} the incident pressure decays to the ambient value in time to which is the positive phase duration. This is followed by a negative phase with a duration t_o- that is usually much longer than the positive phase and characterized by a negative pressure (below ambient pressure) having a maximum value of P_{so}- as well as a reversal of the particle flow. The negative phase is usually less important in a design than is the positive phase, and its amplitude P_s- must, in all cases, be less than ambient atmosphere pressure p_o.

13

The incident impulse density associated with the blast wave is the integrated area under the pressure-time curve and is denoted as is for the positive phase and is for the negative phase.

The above treatment of the blast wave phenomena is general. The magnitude of the various parameters is presented depending upon the category of the detonation. Air burst, free air burst, surface burst which are unconfined explosions are studied in following sections.

2.2.5 Craters Generated By the Blast Waves

In case of terrorist attacks or other intentional actions using explosives, it is extremely important that the information can be obtained from the crater generated by the blast waves. For example, the focus of the explosion and the mass of the explosive used in the attack can be deduced examining the location and dimensions of the crater. However, studies about craters produced by explosions on or above ground level, which would be the case when the explosive charge is situated in a vehicle, are rarely found in the open technical literature [21].

Years of industrial and military experience have been condensed in charts or equations. These are useful tools, for example, to establish the explosive weight to yield a perforation of certain dimensions or to estimate the type and amount of explosive used in a terrorist attack, from the damage registered [21].

A crater produced by an explosive charge situated on or above the ground level is schematized in Figure 2.5. The crater dimensions defined by Kinney and Graham are D is the apparent crater diameter, D_r is the actual crater diameter and H_2 is the apparent depth of the crater [21] (Figure 2.5).
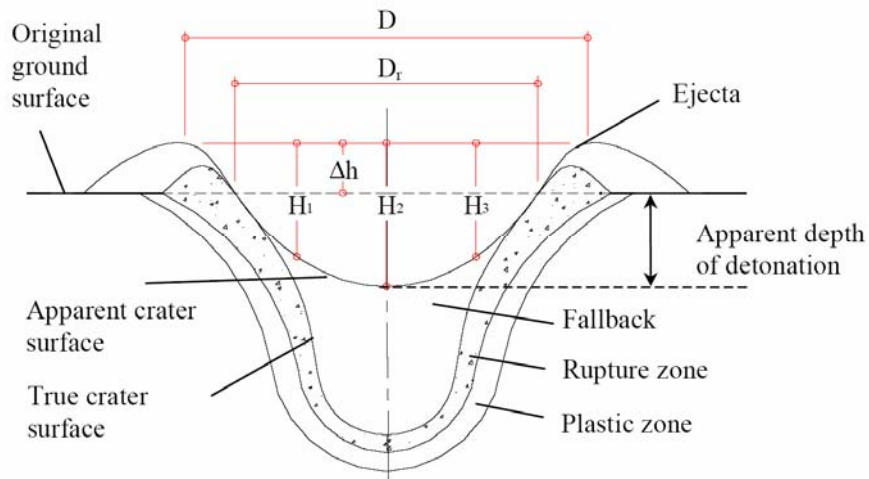
Figure 2.5 Definitions of the crater dimensions [21]

There is less information about explosions at ground level. Statistical studies of about 200 accidental above-ground explosions of relative large magnitude are presented by Kinney and Graham. The results exhibit a variation coefficient in the crater diameter of about 30%. From these results, the following empirical equation for the crater diameter was proposed [21].

$$D[m] = 0.8W[kg]^{1/3} \tag{11}$$

Ambrossini and Luccioni developed the numerical models as well as the analysis procedure which were validated against experimental observations of the crater diameters. They considered influence of soil properties which are shear modulus, mass density, failure criteria and yield strength. They represent the linear approximation of numerical result by minimum least-fit squares. The variation of $\pm 5\%$ accounts for the differences between soil properties that could be found in different sites. Following equations can be proposed for the prediction of crater dimensions in cases (a) and (b) respectively.

Case (a) $D[m] = 0.5W[kg]^{1/3} \pm 5\%$ [21]   (12)

Case(b) $D[m] = 0.65W[kg]^{1/3} \pm 5\%$ [21]   (13)

2.3 BLAST LOADING EFFECT ON STRUCTURES

2.3.1   Technical Design Manuals for Blast-Resistant Design

There are several military design manuals to predict blast loads and the responses of structural systems. Although these design guidelines were focused on military applications they are relevant for civil design practice.

- Structures to Resist the Effects of Accidental Explosions, TM 5-1300 (U.S. Departments of the Army, The Navy, and The Air Force, 1990)

This manual is most widely used publication by both military and civilian organizations for designing structures to prevent the propagation of explosion and to provide protection for personnel and valuable equipment [1].

- A Manual for the Prediction of Blast and Fragment Loadings on Structures, DOE/TIC 11268 (U.S. Department of Energy, 1992)

This manual provides guidance to the designers of facilities subject to accidental explosions and aids in the assessment of the explosion-resistant capabilities of existing buildings [1].

- Protective Construction Design Manual, ESL-TR-87-57 (Air Force Engineering and Services Center, 1989)

This manual provides procedures for the analysis and design of protective structures exposed to the effects of conventional (non-nuclear) weapons and is intended for use by engineers with basic knowledge of weapons effects, structural dynamics, and hardened protective structures [1].

- Fundamentals of Protective Design for Conventional Weapons, TM 5-855-1 (U.S. Department of the Army, 1986)

This manual provides procedures for the design and analysis of protective structures subjected to the effects of conventional weapons. It is intended for use by engineers involved in designing hardened facilities [1].

- The Design and Analysis of Hardened Structures to Conventional Weapons Effects (DAHS CWE, 1998)

This new Joint Services manual, written by a team of more than 200 experts in conventional weapons and protective structures engineering, supersedes U.S. Department of the Army TM 5-855-1, Fundamentals of Protective Design for Conventional Weapons (1986), and Air Force Engineering and Services Centre ESL-TR-87 57, Protective Construction Design Manual (1989) [1].

- Structural Design for Physical Security State of the Practice Report (ASCE, 1995)

This report is intended to be a comprehensive guide for civilian designers and planners who wish to incorporate physical security considerations into their designs or building retrofit efforts [1].

2.3.2 Forces Acting On Structure

The forces acting on a structure associated with a plane shock wave are dependent upon both the peak pressure and the impulse of the incident and dynamic pressures acting in the free-field.

For each pressure range there is a particle or wind velocity associated with the blast wave that causes a dynamic pressure on objects in the path of the wave. In the free field, these dynamic pressures are essentially functions of the air density and particle velocity. For typical conditions, standard relationships have been established between the peak incident pressure (P_{so}), the peak dynamic pressure (q_o), the particle velocity, and the air density behind the shock front. The magnitude of the dynamic pressures, particle velocity and air

density is solely a function of the peak incident pressure, and, therefore, independent of the explosion size.

For design purposes, it is necessary to establish the variation or decay of both the incident and dynamic pressures with time since the effects on the structure subjected to a blast loading depend upon the intensity-time history of the loading as well as on the peak intensity. The form of the incident blast wave (Figure 2.6) is characterized by an abrupt rise in pressure to a peak value, a period of decay to ambient pressure and a period in which the pressure drops below ambient (negative pressure phase).
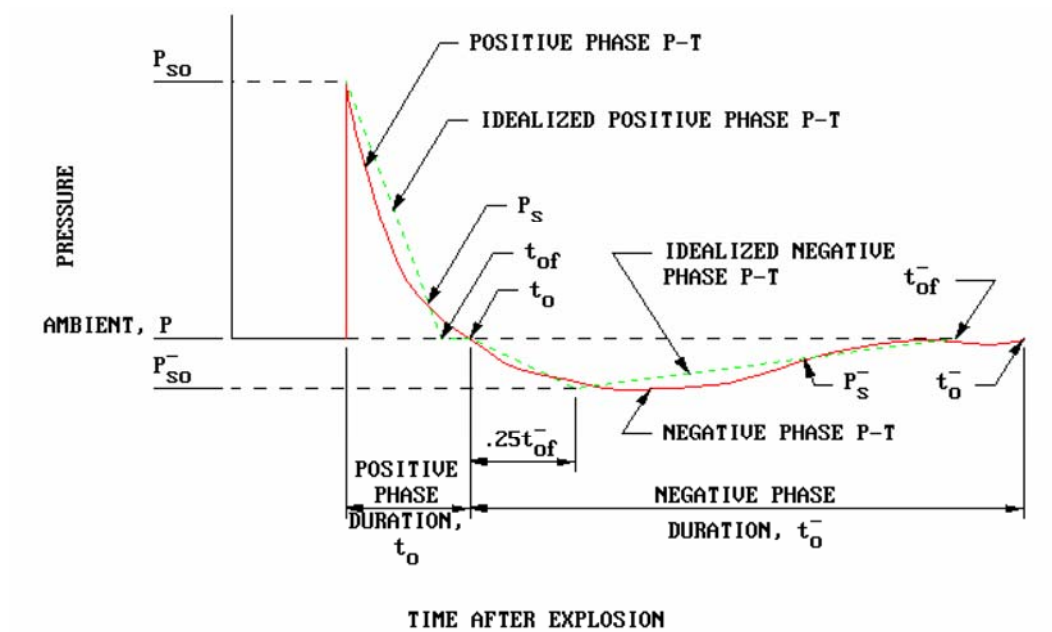
Figure 2.6 Idealized pressure-time variation [3]

The rate of decay of the incident and dynamic pressures, after the passage of the shock front, is a function of the peak pressure (both positive and negative phases) and the size of the detonation. For design purposes, the actual decay of

the incidental pressure may be approximated by the rise of an equivalent triangular pressure pulse. The actual positive duration is replaced by a fictitious duration which is expressed as a function of the total positive impulse and peak pressure:

$$t_o = 2i / p \tag{14}$$

The above relationship for the equivalent triangular pulse is applicable to the incident as well as the reflected pressures; however, in the case of the latter, the value of the pressure and impulse used with equation (14) is equivalent to that associated with the reflected wave. The fictitious duration of the dynamic pressure may be assumed to be equal to that of the incident pressure.

For determining the pressure-time data for the negative phase, a similar procedure as used in the evaluation of the idealized positive phase may be utilized. The equivalent negative pressure-time curve will have a time of rise equal to 0.25 to whereas the fictitious duration t_{of}^- is given by the triangular equivalent pulse equation:

$$t_{of}^- = 2i^- / p^- \tag{15}$$

where i^- and p^- are the total impulse and peak pressure of the negative pulse of either the incident or reflected waves. The effects of the dynamic pressure in the magazine phase region usually may be neglected.

Since the fictitious duration of the positive phase will be smaller in magnitude than the actual duration, a time gap will occur between the fictitious duration and the onset of the negative phase. This time gap, which is illustrated in Figure 2.6, should be maintained in an analysis for consistency of the onset of the various load phases [3].

19

2.3.3 Blast-Loading Categories

Blast loads on structures may be classified into two main groups based on the confinement of the explosive charge (unconfined and confined explosions). These blast loading categories are illustrated in Table 2.3. Table 2.3 gives the six blast loading categories possible. Table 2.3 also shows the five possible pressure loads (Unreflected, reflected etc.) depended on the blast load categories.

Table 2.3 Blast Loading Categories [3]

BLAST LOADING CATEGORIES		
CHARGE CONFINEMENT	**CATEGORY**	**PRESSURE LOADS**
Unconfined Explosions	Free Air Burst	Unreflected
	Air Burst	Reflected
	Surface Burst	Reflected
Confined Explosions	Fully Vented	Internal Shock
		Leakage
	Partially Confined	Internal Shock
		Internal Gas
		Leakage
	Fully Confined	Internal Shock
		Internal Gas

The blast load categories and the resulting pressure loads are defined below.

2.3.3.1 Unconfined Explosion

2.3.3.1.1 Free Air Burst

If the explosive source is above the structure or adjacent to the structure, and there is no change in initial shock wave, then the blast loads acting on the structure are free-air blast pressures (Figure 2.7).
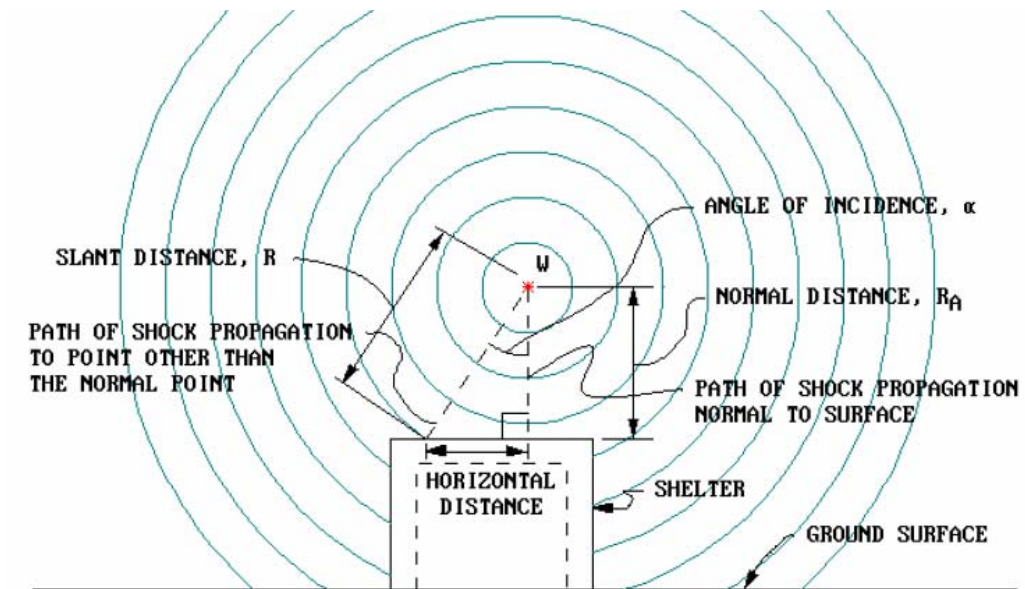
Figure 2.7 Free-air burst blast environment [3]

The pressure and impulse occurs as a result of an explosion and is reinforced and reflected when the incident wave impacts with the structure (Figure 2.8).

When the shock wave reaches a surface on the path of travel that on the wave is normal to the surface, then at the point of initial contact, maximum pressure and impulse are sustained.

The peak pressure and impulse patterns on the structure vary with distance from a maximum at the normal distance R_A to a minimum (incident pressure) where the plane of the structure's surface is perpendicular to the shock front. The positive phase pressures, impulses, durations, and other parameters of this shock environment for a spherical TNT explosions are given in Figure 2.9 versus the scaled distance ($Z = R/W^{1/3}$).
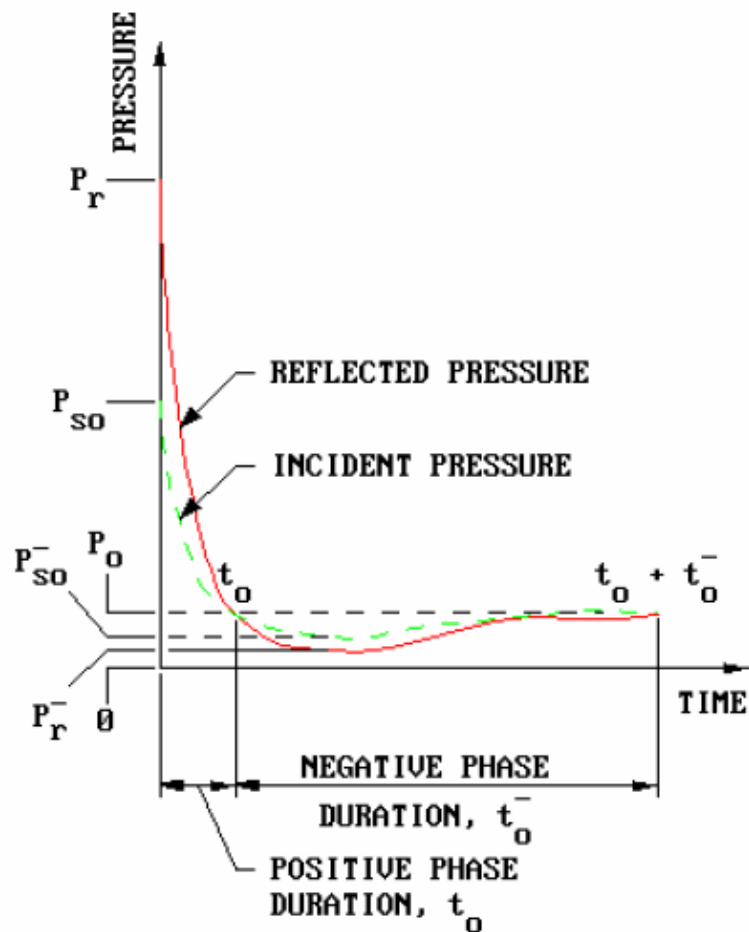
Figure 2.8 Pressure-time variation for a free-air burst [3]

The dashed portions of the curves are the parameters which have been extrapolated. These dashed curves represent an upper limit of scatter in experimental data and variation in theoretical predictions in order to give for design purposes conservative limits.

Usually negative blast wave parameters are used for flexible structures such as made of steel. The effects of the negative phase parameters are usually not important for the design of the more rigid type structures (reinforced concrete) because maximum pressure may damage structure no recoverably.
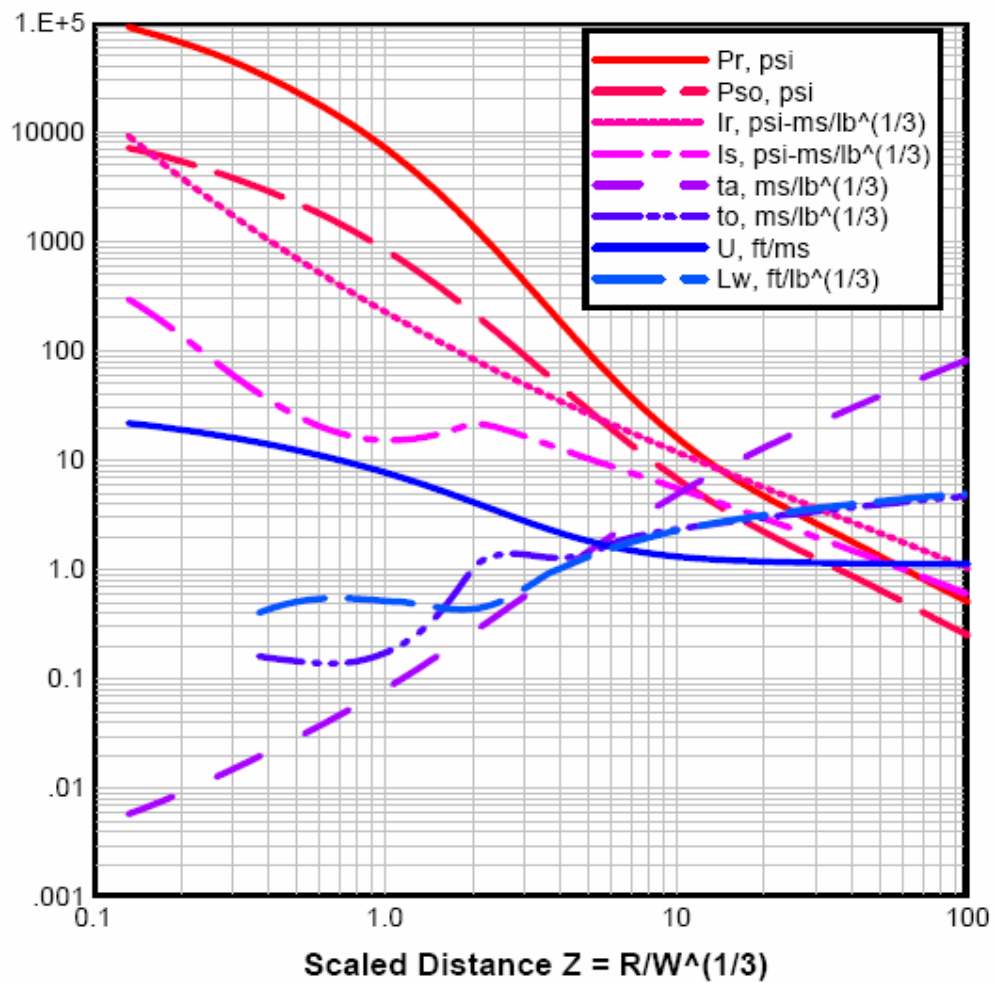
Figure 2.9 Positive phase shock wave parameters for a spherical TNT explosion in free air at sea level [3]

The variation of the pressure and impulse patterns on the surface of a structure between the maximum and minimum values is a function of the angle of incidence. The effects of the angle of incidence on the peak reflected pressure P_{ra} and the reflected impulse i_{ra} are shown in Figure 2.10 and Figure 2.11. The figures are plots of the angle of incidence versus the peak reflected pressure or the reflected impulse as a function of the scaled normal distance between the charge and the surface.

23
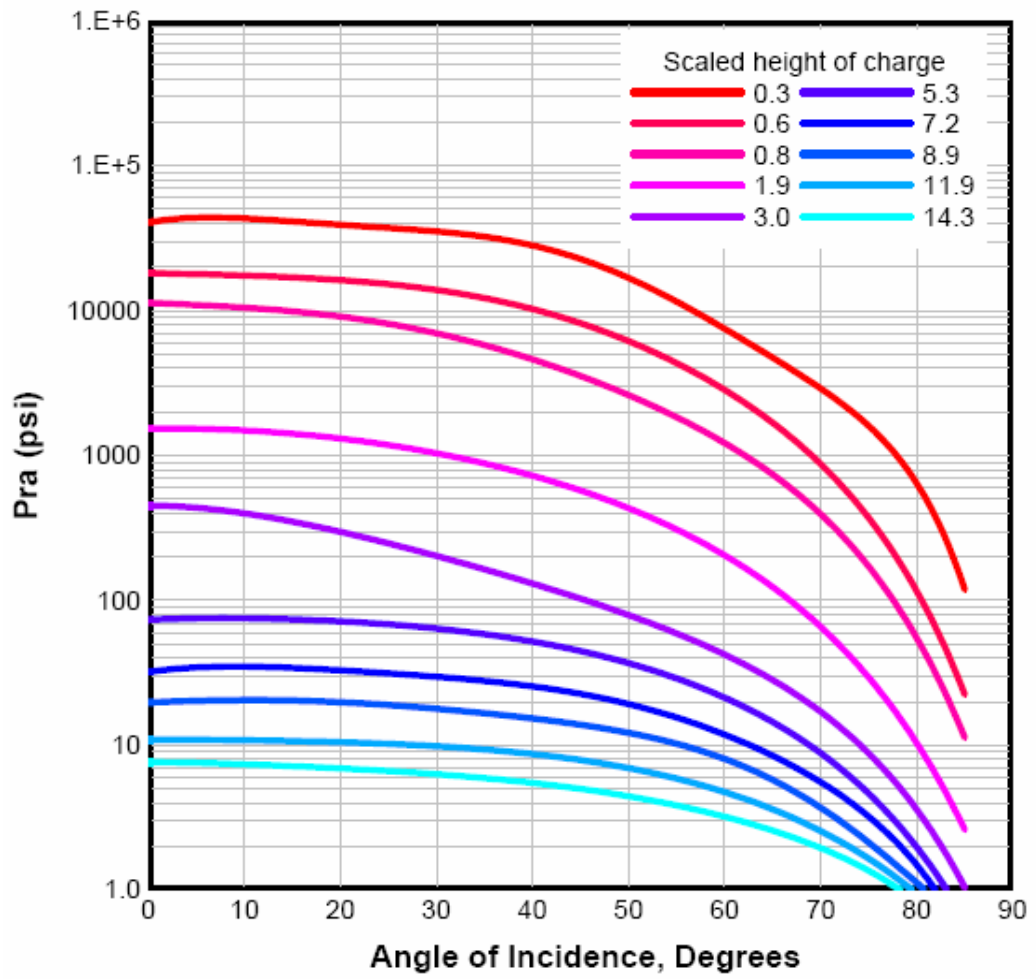
Figure 2.10 Variation of reflected pressure as a function of angle of incidence[3]
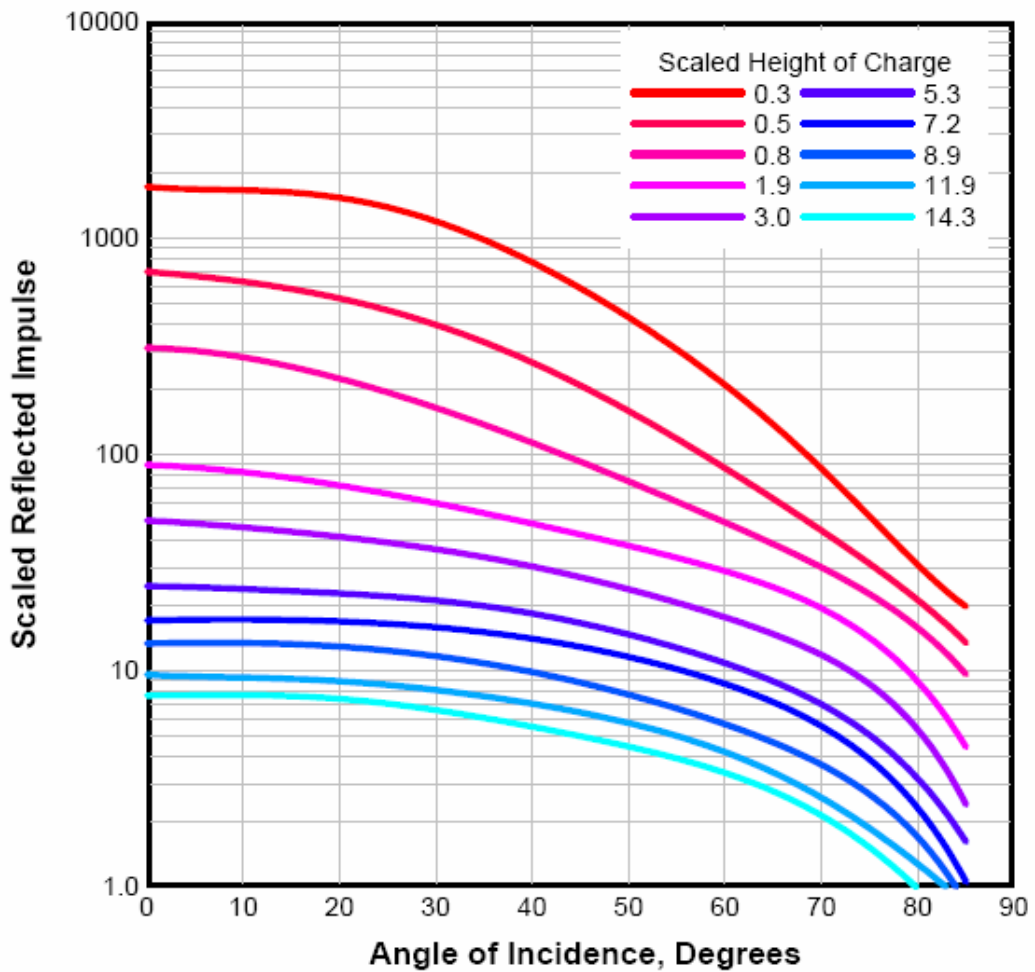
Figure 2.11 Variation of scaled reflected impulse as a function of angle of incidence [3]

2.3.3.1.2 Air Burst

If the explosive source is above the ground surface and at a distance away from the protective structure so that the initial shock wave impinges on the ground surface prior to arrival at the structure then the blast loads acting on the structure are air blast pressures.

As the shock wave continues to propagate outward along the ground surface, a front known as the Mach front (Figure 2.12) is formed by the interaction of the

initial wave (incident wave) and the reflected wave. This reflected wave is the result of the reinforcement of the incident wave by the ground surface.
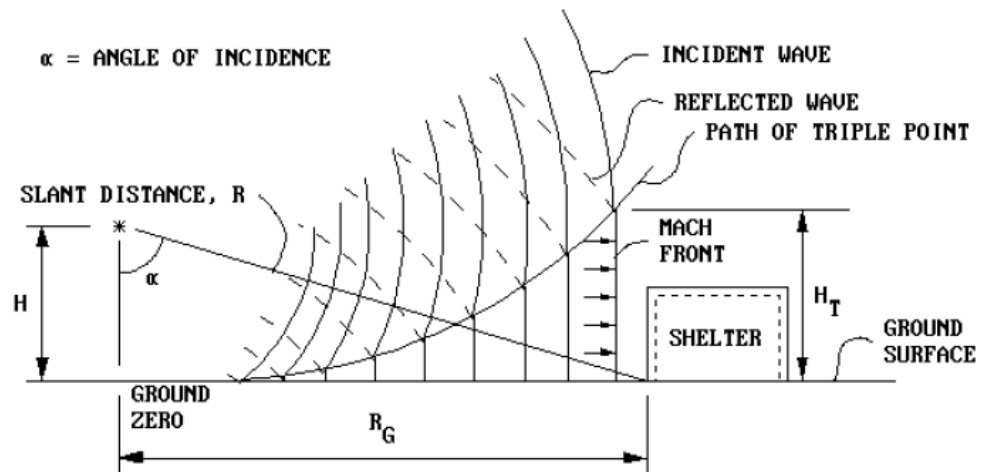
Figure 2.12 Air burst blast environment [3]

The blast parameters in the Mach front are calculated at the ground surface. At the Mach front, the pressure-time variation is similar to that of the incident wave but the blast parameters are larger.

The height of the Mach front increases as the wave propagates away from the center of the detonation in the path of triple point. This increase is the intersection of the initial, reflected, and Mach waves.
When the height of the triple point exceeds the height of the structure, the structure is subjected to uniform pressure. The magnitude of pressures above the triple point is smaller than that of the Mach front.

In determining the magnitude of the air blast loads acting on the surface of an above-ground protective structure, the peak incident pressure P_{ra} is determined from Figure 2.10 using the scaled height of charge above the ground $H_c/W^{1/3}$

26

and the angle of incidence a. The impulse i_{ra} is determined from Figure 2.11 by using similar procedure.

If it is estimated that P_{ra} and i_{ra} are equal to the values of the peak incident pressure P_{so} and incident impulse, other parameters P_r, P_{so}^-, $t_A/W^{1/3}$, U, $L_W/W^{1/3}$ and $L_W^-/W^{1/3}$ can be obtained from Figure 2.9.

2.3.3.1.3 Surface Burst

If the charge is located on or very near the ground surface, it is considered to be a surface burst. The initial wave of the explosion is reflected and reinforced by the ground surface to produce a reflected wave. The reflected wave merges with the incident wave at the point of detonation to form a single wave, hemispherical in shape (Figure 2.13).
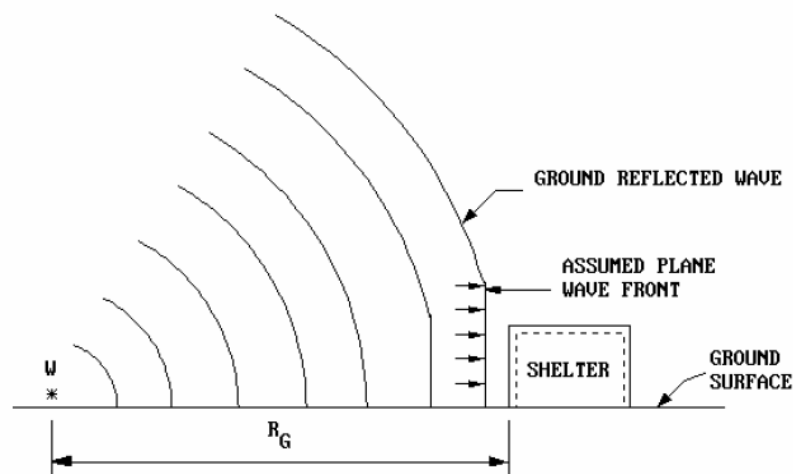
Figure 2.13 Surface burst blast environment [3]

The positive phase parameters are given in Figure 2.14.

27
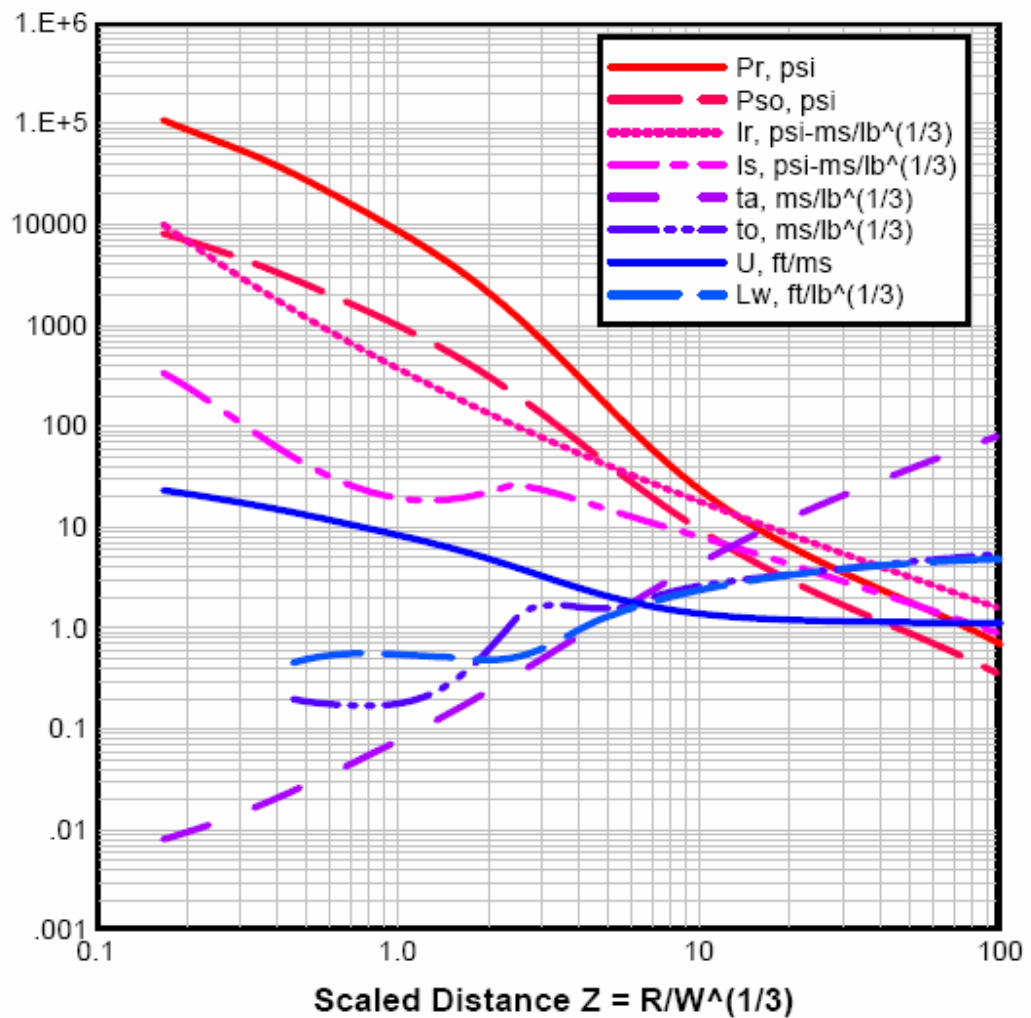
Figure 2.14 Positive phase shock wave parameters for a hemispherical TNT explosion the surface at sea level [3]

An estimate of the blast parameters other than incident pressure and impulse may be obtained from Figure 2.14. The scaled ground distance corresponding to the incident pressure P_{so} is used to obtain the values of P_r, P_{so}^-, P_r^-, $t_A/W^{1/3}$, U, $L_w/W^{1/3}$ and $L_W^-/W^{1/3}$. In addition, this scaled ground distance $Z_G = R_G/W^{1/3}$ is used to calculate the equivalent TNT design charge weight W for pressure using the actual ground distance R_G.

2.3.3.2 Confined Explosion

2.3.3.2.1 Fully Vented Explosion

If the explosion is produced within or adjacent to a barrier or cubicle type structure with one or more surfaces open to the atmosphere, it is a fully vented explosion.

2.3.3.2.2 Partially Confined Explosion

If the explosion is produced within a barrier or cubicle type structure with limited size openings and/or frangible surfaces, it is a partially confined explosion.

2.3.3.2.3 Fully Confined Explosions

If the explosion is produced within either total or near total containment, it is fully confined explosion.

2.3.4 Air Blast Shock Wave inside Structure

The blast load phenomena have been discussed in previous chapters. But it is also important to understand the structural response as well as understanding the loading characteristics. Since blast load is a dynamic load and dissipates in forms of waves, it may develop extraordinary effects rather than the other loading types.

Damage due to the air-blast shock wave may be divided into direct air-blast effects and progressive collapse. Direct air-blast effects are damage caused by high-intensity pressures of air blast close to the explosion. These may induce localized failure of exterior walls, windows, roof systems, floor systems, and columns. Progressive collapse refers to the spread of an initial local failure from element to element, eventually resulting in disproportionate extent of collapse relative to the zone of initial damage. Localized damage due to direct air-blast effects mat or may not progress, depending on the design and

construction of the building. To produce a progressive collapse, the weapon must be in close proximity to a critical load-bearing element. Progressive collapse can propagate vertically upward or downward from the source of explosion, and it can propagate laterally from bay to bay as well [10].

The shock wave also acts in directions that the building may not have been designed for, such as upward pressure on the floor system. In terms of sequence of response, the air blast first impinges the exterior envelope of the building. The pressure wave pushes on the exterior walls and may cause wall failure and window breakage. As the shock wave continues to expand, it enters the structure, pushing both upward on the ceilings and downward on the floors (Figure 2.15). Floor failure is common in large-scale vehicle-delivered explosive attacks, because floor slabs typically have a large surface area for the pressure to act on and a comparably small thickness [10].
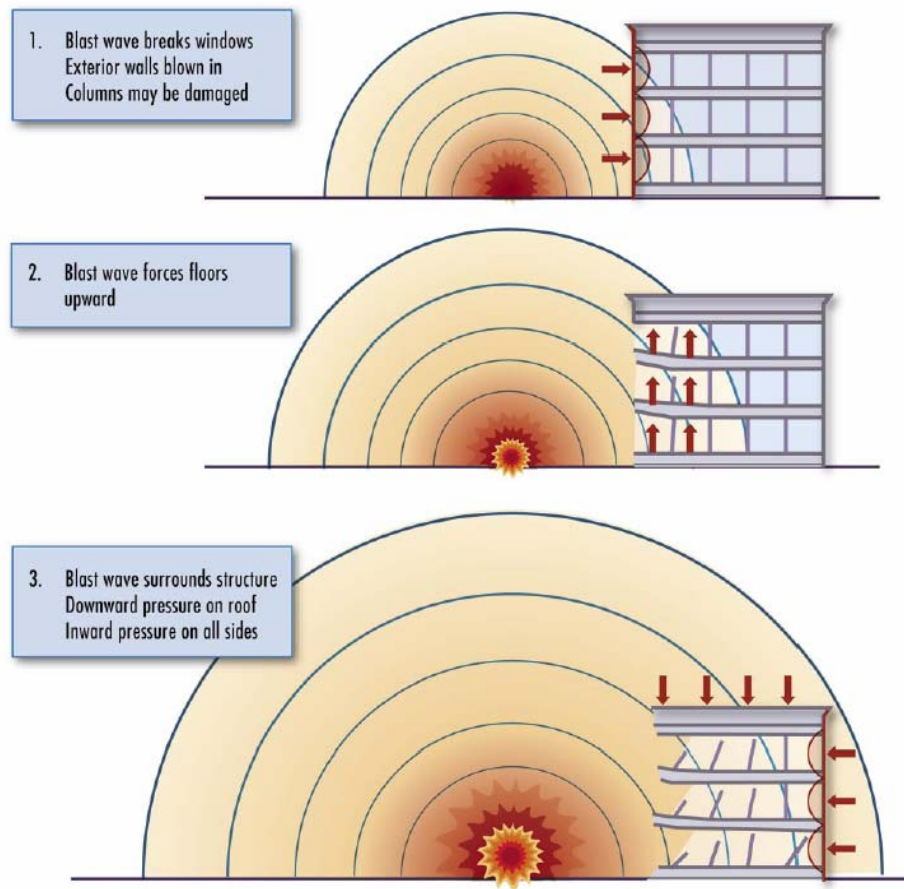
Figure 2.15 Blast pressure effects on a structure [10]

2.3.5 Computer Programs

There are several computer programs to calculate blast loads and their influence to the structures. Examples of the programs are BLASTX, CTH, FEFLO, FOIL, SHARC, DYNA3D, ALE3D, LS-DYNA, Air3D, CONWEP, AUTO-DYN, ABAQUS, ATBLAST, SBEDS. Atblast and Sbeds are chosen to define in this thesis because they are most noticed programs in use.

- SBEDS (Single Degree of Freedom Blast Effects Design Spreadsheets)

The SBEDS workbook is an Excel-based tool for design of structural components subjected to dynamic loads using single degree of freedom

(SDOF) methodology. It was developed by for the U.S. Army Corps of Engineers Protective Design Center as a tool for designers to use in satisfying Department of Defense (DoD) antiterrorism standards.

SBEDS allows the user to choose from 10 common structural components and enter readily available parameters related to material properties and geometry and allow the workbook to calculate the SDOF properties or directly enter the SDOF properties. SBEDS follows the guidance contained in Army TM 5-1300, "Structures to Resist the Effects of Accidental Explosions", and Unified Fatalities Criteria (UFC) 3-340-0 (FOUO), "Design and Analysis of Hardened Structures to Conventional Weapons Effects", as applicable [8].

- AT-BLAST

AT-Blast is a software program that estimates the blast loads that develop during an open-air explosion. The program allows the user to input minimum and maximum range, explosive charge weight, and angle of incidence. From this information, AT-Blast calculates the following values: shock front velocity, time of arrival, pressure, impulse, and duration. AT-Blast is a proprietary computer program developed by Applied Research Associates, Inc. and is provided at no cost to the government and to authorized users [9].

2.4 RECOMMENDATIONS (STRENGTHENING)

2.4.1 Wall/Fence Protection

One of the simplest and most effective ways of providing protection to an existing building is to keep the source of the blast loading at as long a range as possible. Creation of even a modest stand-off distance will mean that blast loading on the building is much reduced in comparison with a close-in blast, because blast resultants decrease rapidly with increased range. Stand-off can be

achieved by locating the building remote from property boundaries, and stand-off can be maintained by denying access to potential vehicle bombs by the use of robust bollards or 'planters'' capable of stopping even a fairly fast moving vehicle from getting close to the building. Figure 2.16 shows a schematic layout of a site for protection against vehicle bombs [2].
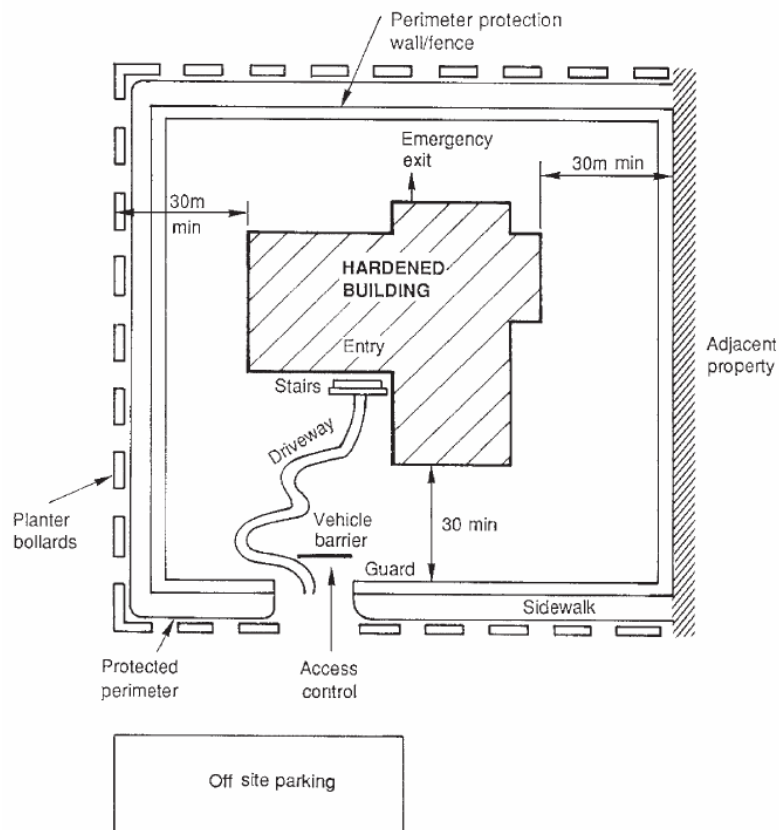
Figure 2.16 Schematic layout of site for protection against vehicle bombs [2]

2.4.2   CFRP Protection

Reinforced concrete (RC) columns strengthened using composite wrap will lessen the risks of progressive collapse due to terrorist attacks and earthquakes. Full-scale blast and laboratory tests have verified that the behavior of existing

33

non-ductile RC columns can be substantially upgraded by simply wrapping them with carbon fiber reinforced polymer (CFRP) [20].

Wrapping a typical East Coast RC column with a carbon fabric impregnated with a polymer changes its often brittle behavior to a highly ductile one as well as increases the strength of the column. Figure 2.17 and Figure 2.18 show analytic results that illustrate the kind of before and after wrap behavior that may be expected of these types of office building columns—that is, ones typically found on the East Coast or other regions of low seismic activity. [20]

Carbon fiber reinforced polymer (CFRP) has been used in a variety of applications to strengthen and add ductility to RC and masonry components.
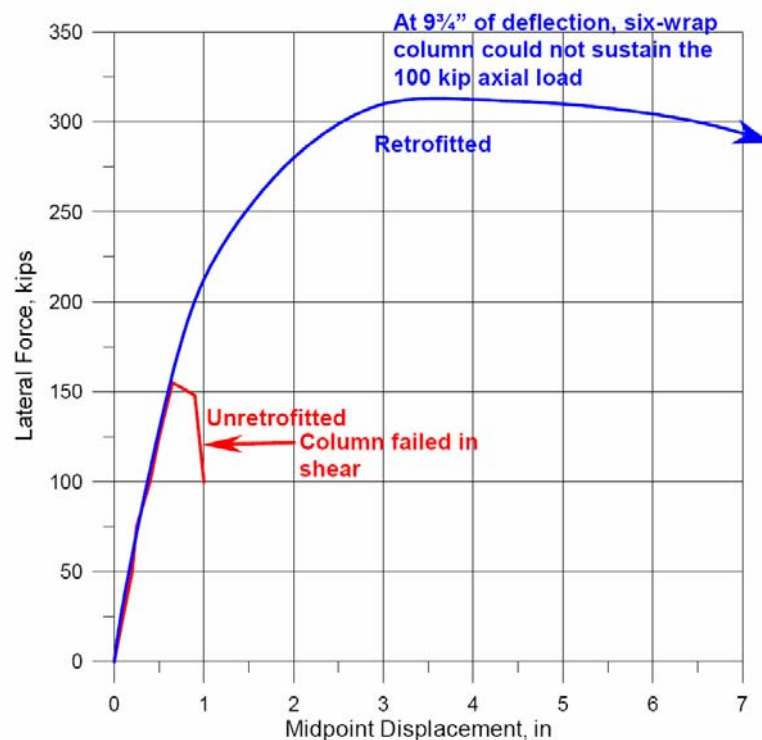
Figure 2.17 Midpoint displacement vs. lateral force: comparisons between retrofitted and unretrofitted column [20]

(a) Non-ductile shear failure behavior of as is column.

(b) Markedly ductile behavior afforded by CFRP hoop wrap.

Figure 2.18 Behavior under statically applied simulated blast load for RC columns typical of an East Coast building [20]

Composite wrap provides several benefits. First, it increases the diagonal shear resistance of the column so as to ensure the column responds in a ductile flexure mode. Second, it enlarges the zones over which the plastic hinges occur at the column's ends and middle and strengthens the concrete in this area to ensure that the hinging is related to yielding of the rebar (i.e., a plastic hinge). Because of hardening, this will cause the hinge to spread out, which increases energy absorption and ductility. Finally, CFRP substantially increases the column's deflection limit; this limit indicates when the column is no longer able to carry its axial load (Figure 2.18) [20].

CHAPTER 3

ANALYTICAL MODELING

3.1 NEED FOR BLAST LOADING ANALYSIS

Blast loading has several parameters defining the pressure level being exerted on the building and time interval (duration) of pressure loading. Available charts to define loading on the structure are mostly developed for TNT; however, other types of explosives (such as C4, A4, ammonium nitrate, etc) can be defined in terms of TNT equivalence. Once the loading conditions are defined for a selected explosion scenario, the response of a structure to that loading should be investigated. Since the explosion loading takes place in a very short duration of time, the response of the structure to that loading is far different from static loading analysis. The dynamic properties of the structure and structural members also play an important role on the response of a structure. The post-loading response of a building is another important aspect of the structural response, since failure of a column might generate a sequential collapse mechanism of the supported floors above that column. Therefore, observation of real life bomb attacks is necessary to understand the nature of structural behavior and the need for analytical modeling and analysis.

3.2 GLOBAL CASES

Two case scenarios are given below for attacks on Alfred P. Murrah Federal Building, in Oklahoma, USA and Argentina-Israeli Mutual Association, AMIA Building, at Buenos Aires, Argentina.

3.2.1   Attack on Alfred P. Murrah Federal Building, OKLAHOMA, USA

On April 19, 1995, a truck loaded with an ammonium nitrate and fuel oil bomb caused collapse of fully half of the total floor area of the nine-story, reinforced concrete Murrah Federal Building in Oklahoma City. 168 people including 19 children and one rescue worker were killed. The extent of the collapse, which extended well beyond the zone of direct structural blast damage, prompted studies of progressive/disproportionate collapse and development of new design guidelines for important buildings.

The Murrah Building was a nine-story, conventionally reinforced (nonductile), concrete structure constructed during the mid-1970s.

The truck bomb, estimated to be 1,800 kg (4,000 lb) TNT equivalent, was centered approximately 4 m (13 ft) from Column G20, as shown graphically in Figure 3.1. Given its proximity to the blast, it is generally believed that the concrete of Column G20 was shattered by the blast, leaving only the column's bundled reinforcing steel. Absent any alternative load path, loss of Column G20 led to the loss of four bays over the full height of the building, as shown in Figure 3.1.

As the blast wave expanded, it exerted an upward force on the floor slabs. As the 152 mm (6 in.) thick floor slabs were relatively light [3.6 kPa (75 psf)] and not reinforced to resist upward pressures. Once the blast wave passed, gravity took over, beam/column connections failed in punching shear, and the floor structure draped as a catenary, as shown in Figure 3.2.

Destruction of the Murrah Building was a combination of direct blast effects that destroyed one column and large portions of the second-, third-, and perhaps portions of the fourth-floor slab [4].

37
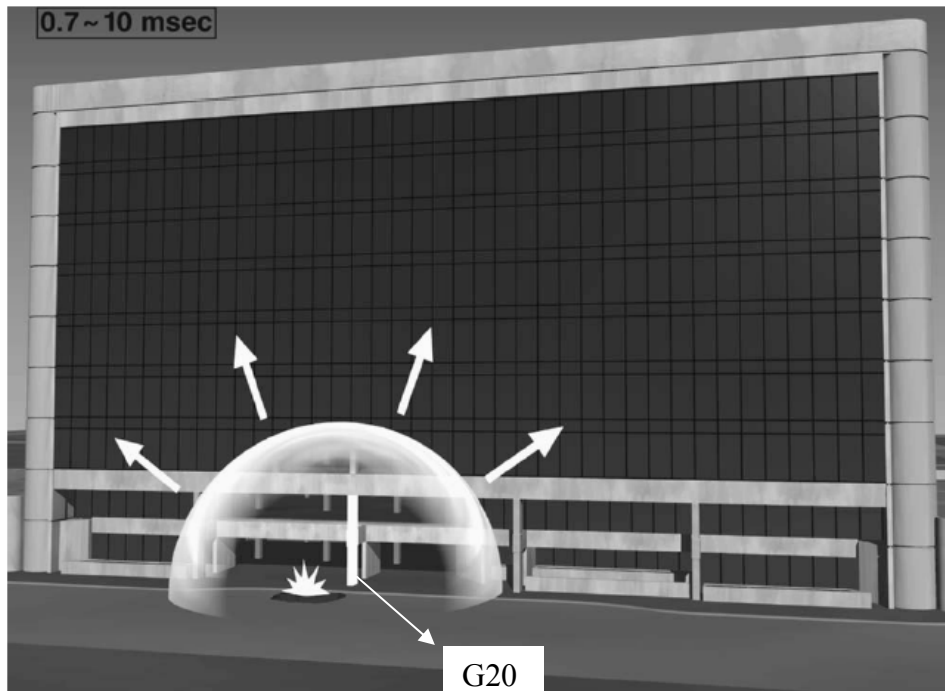
Figure 3.1 Isometric view showing location of blast relative to building structure [4]
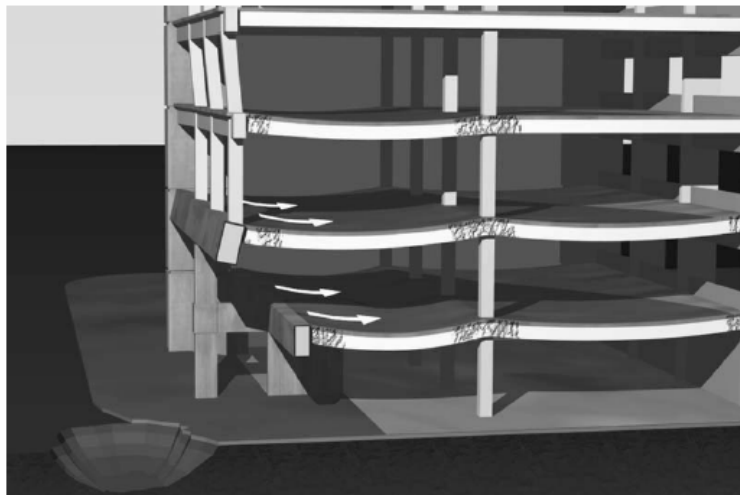
Figure 3.2 Illustration of catenary action of floor slab and beams following punching shear failure at columns [4]

Figure 3.3 Attack on Alfred P. Murrah Federal Building, Oklahoma, ABD [6]

3.2.2 Attack on the Argentina-Israeli Mutual Association, AMIA Building- Buenos Aires, ARGENTINA

On July 18, 1997, a powerful bomb made of ammonium nitrate was driven in a van through the front gates of AMIA building in the Once district near downtown Buenos Aires. The building was a seven-story structure which was the headquarters of Argentina's Jewish community (Figure 3.4). 85 people were killed and more than 300 others were wounded.

It is assumed that the damage was caused by an explosive load equivalent to 400 kg of TNT placed in the entrance hall of the building. The results obtained for an explosive load of 400 kg of TNT located 1 m above the ground level, 1 m inside the entrance hall and 1 m to the right of the axis of the building are shown in Figure 3.4.
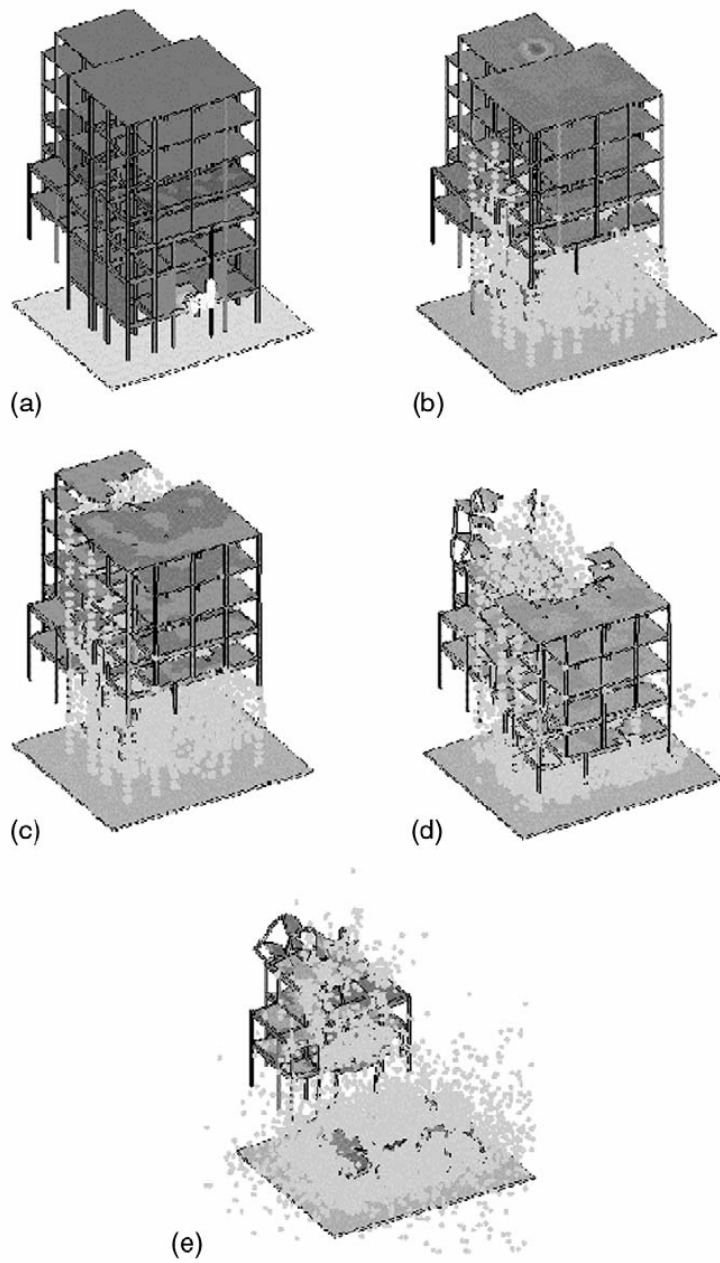
Figure 3.4 Evolution of damage produced by the explosion (model of AUTODYN) (a) 0.75 ms, (b) 254 ms, (c) 378 ms, (d) 1350 ms, (e) 2460 ms [5]

Figure 3.5 Attack on the Argentina-Israeli Mutual Association [7]

The structural collapse was due to a gravitational mechanism produced by the failure of most of the load bearing columns of the first stage in the front block. See Figure 3.4.

The first three lines of columns of the underground level and the first level resulted almost completely destroyed (Figure 3.4b) leaving without support the upper floors that began to fall down pulling from the back block (Figure 3.4c). Beams and columns in the upper floors of the intermediate block have failed by a combination of tension, flexure and shear [5].

It is clear that in attacking on the AMIA Building, the collapse was due to a gravitational mechanism originated by the destruction of the lower columns.

3.3 VULNERABILITY ASSESSMENT

As seen in the global cases, most attacks that use explosives which threaten the structures are carried out by humans (suicide bombers) or aerial vehicles.

Therefore, the lowermost columns of the structure, which are also the most critical elements, are the most susceptible ones to damage. On the other hand, internal blast or airplane collapse to upper or middle floors of high rise buildings may also be critical as the upper stories mass falls down and crashes over the lower floors, the whole building may collapse (e.g., world trade center collapse). This study concentrates on exterior bombs or explosions at the ground level.

Damage suffered by an exterior column most likely leads to the collapse of at least the section of the building above the failed column. This is because of the destruction of the supports of the beams and slabs, resulting in a reversed bending moment at column beam junction and doubled span length that needs to be carried by the beams. The excessive pressure that is created by an explosion can cause large amount of damage, even if small amounts of explosives are used.

In the attacks that use explosives, the pressure level created by explosion deviates very rapidly and inversely as a function of distance. Members at the close proximity of explosion are highly susceptible to damage rather than the whole structure itself; therefore, particular members of the structure are primarily influenced. Extensive amounts and effective positioning of explosives are needed in order to create an effective loading to the collapse of whole structure. For this reason, behavior of a single reinforced concrete column under blast effect was studied under the scope of this thesis. Although load redistribution would take place in a statically indeterminate system, it was assumed that in the case of reinforced concrete frame type buildings, collapse of a ground floor column would lead to partial collapse of the building above that column. General assumptions including the effect of column failure to the rest of the building are listed and discussed in the following section.

3.4 GENERAL ASSUMPTIONS

Some assumptions were made in order to perform the performance evaluation of R/C columns in the scope of this thesis. The assumptions tried to be kept reasonable in the context of engineering while making the analysis manageable.

The assumptions and brief reasons are explained below,

1. In this thesis, a reinforced concrete column was analyzed under blast load. The column was assumed to be the first floor column having foundation at the bottom end and beam-column joint at the top end. Both ends were assumed to be fixed ends, since the blast load would also try to bend the upper storey column inwards generating an almost zero rotation at the support. Furthermore, torsional and bending resistance of the joining beams as well as the slab would generate a certain level of fixity when compared with the rotational stiffness of the columns.
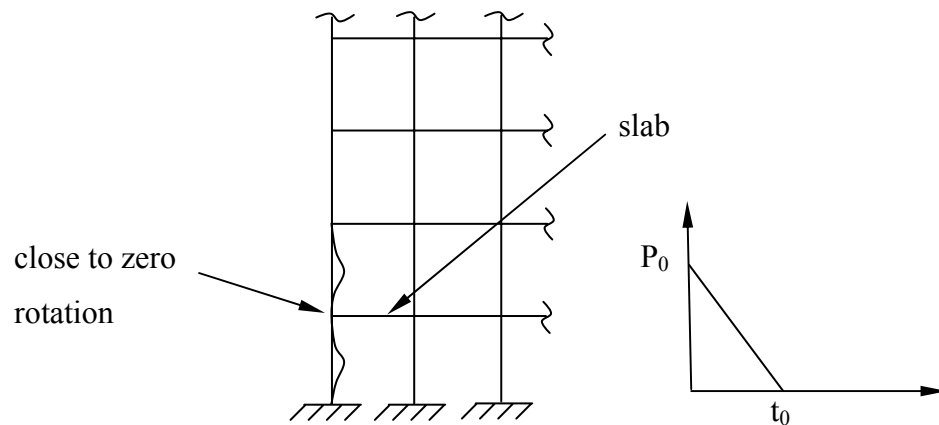
Figure 3.6 Typical section of a structure and pressure versus time variation

If we consider the slab,
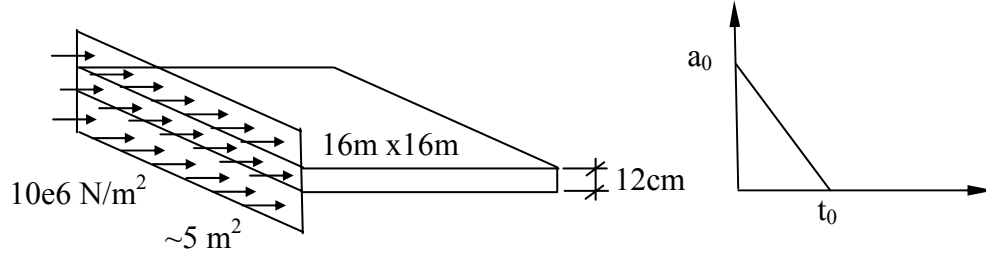
Figure 3.7 Typical blast load distribution of a concrete slab and acceleration versus time variation

$P_0 \cong 10 MPa$

$t_0 \cong 3m\sec$

$m = 30.72m^3 \times 2.5t/m^3 = 76.8ton$ (mass)

$a \cong \dfrac{F}{m} = \dfrac{10e6 \times 5m^2}{76.8}/2 = 400m/s^2$ (excluding column stiffness)

If we consider typical pressure-time relationship of blast load shown as above,

$a = a\left(1 - \dfrac{t}{t_0}\right)$

$V = a_0\left(t - \dfrac{t^2}{2t_0}\right)$

$x = a_0\left(\dfrac{t^2}{2} + \dfrac{t^3}{6t_0}\right) (t_0 \to 0)$

$x(t_0) \cong a_0\left(\dfrac{t_0{}^2}{2} + \dfrac{t_0{}^2}{6}\right) = \dfrac{1}{3}at_0{}^2 = \dfrac{1}{3} \times 400 \times (3 \times 10^{-3})^2$

$x(t_0) = 1.2mm \cong 0.034\% << 2\%$ (max drift according to the code)

Including the stiffness contribution of the remaining columns coexist at the same floor of the loaded column; slab movement is negligible due to its large mass, diaphragm action, small surface exposure, etc.

2. Square column cross-section geometry was assumed for the column.

3. The reinforced concrete column was analyzed by using Kent & Park concrete model which includes the effect of confinement. Therefore the spacing of stirrups had direct effect on the analysis results.

4. The spacing and diameter of stirrups were also used to determine the shear capacity (V_n) of the column.

5. The effect of axial column load (P) on the bending moment capacity (Mp) was incorporated to the analysis.

6. Behavior of the column section was assumed to be elastic. If the analysis results indicate that the elastic capacity is exceeded, the output would be deemed invalid and a conclusion can be drawn that the column would fail.
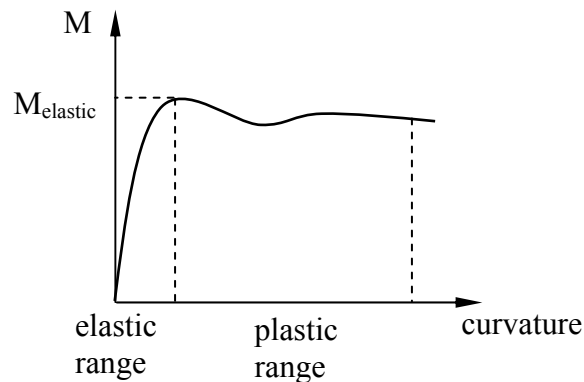
Figure 3.8 Typical Moment-curvature relationship of a concrete column

7. It was found in the literature that columns would commonly reach their shear capacities before a plastic hinge formation mechanism. Therefore, failure of a column by formation of plastic hinges can be expected for very slim and tall columns.

45

8. In order to be able to analyze the behavior of a column under blast load, the characteristics of the loading should be well understood. The characteristics of the blast load dissipation and magnitude were studied with experiments in the literature. After the verification of these experiments, clauses about the blast loads are inserted in to the military specifications. These technical specifications are also accepted as reference documents in academic studies. These specifications are also being used in the analysis and design of civil and public structures. Therefore, the shape and the magnitude of the blast loads used in the analysis of the column in this thesis were accepted and taken from these codes (as defined in the previous chapters).

9. The blast loading is characterized with an instant explosion and then gradually decreasing curve. The duration of the blast pressure is described in terms of milliseconds and has a decreasing shape (not constant). Therefore using dynamic analysis with time step increment assumed to be more realistic and used in this thesis.

10. The blast loading category is assumed to be unconfined air burst which takes into account the mach reflection. This reflected wave is the result of the reinforcement of the incident wave by the ground surface.

11. The negative pressure range of the blast load was not considered in the analysis since a) the natural period of the column is generally shorter than the duration of blast (t_o) generating the peak column displacement before reaching t_o and b) the suction pressure range is commonly ignored in the literature to stay on the conservative side.

12. The strain rate effect is considered in the analysis as it is discussed in section 3.5.6.

13. The amount and the layout of the reinforcement in the section was defined by conjecturing that $\dfrac{N}{A_c} \leq 0.3 f_{ck}$.

3.5 FINITE ELEMENT ANALYSIS

Fundamentally, the behavior of all types of structures – frameworks, plates, shells, or solids – is described by means of differential equations. It has been long established that such structures may be treated as assemblages of one dimensional member [18].

Structures consisting of two or three dimensional components – plates, membranes, shells, solids – are more complicated in that rarely do exact solutions exist for the applicable partial differential equations. One approach to obtaining practical, numerical solutions is the finite element method. The basic concept of the method is that a continuum (the total structure) can be modeled analytically by its subdivision into regions (the finite elements) in each of which the behavior is described by a set of assumed functions representing the stresses or displacements in that region. This permits the problem formulation to be altered to one of the establishment of a system of algebraic equations [18]. This thesis deals with finite element mechanics. Specifically, it is on matrix structural analysis as shown in flow chart (Figure 3.9).
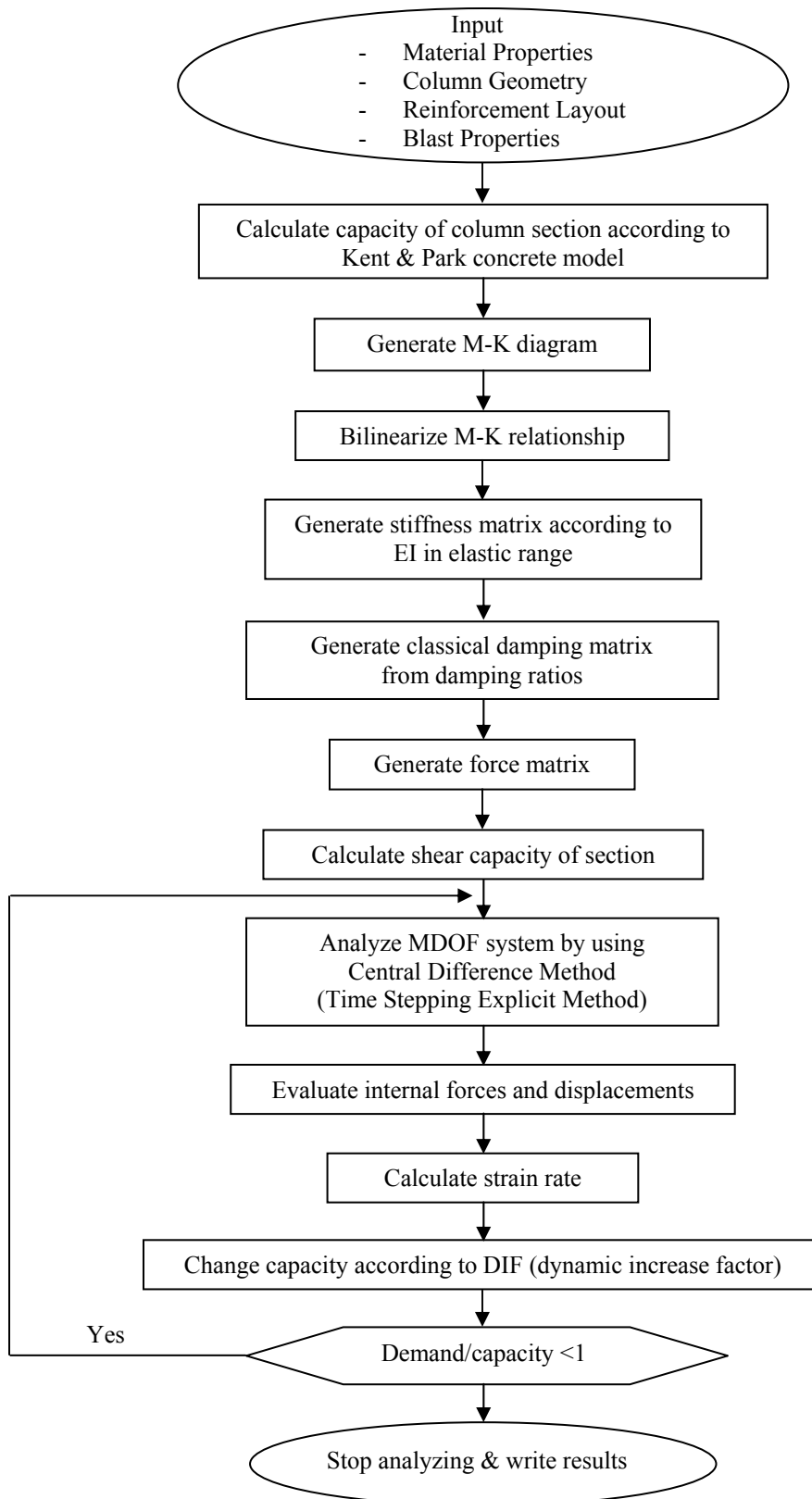
Figure 3.9 Flow chart of the analysis program

3.5.1 Matrix Displacement Method

Displacement method (or stiffness or equilibrium) is used in analyses since we are dealing with linear structure. The displacements and the internal forces are uniquely related one can be obtained from the other. Displacement method of structural analysis relies on the establishment of stiffness equations which are equations relating forces to displacements. In the matrix and finite element displacements methods the equations governing the response of the whole structure to an applied static loading are always in the form of the following equation.

$$F = KD \tag{16}$$

In equation (16), F is the column matrix of (known) applied nodal forces, D is the column matrix of unknown nodal displacements, and K is the structure stiffness matrix.

3.5.1.1   *Construction of Stiffness Matrix*

$$k = \begin{bmatrix} \dfrac{12EI}{l^3} & \dfrac{6EI}{l^2} & \dfrac{-12EL}{l^3} & \dfrac{6EI}{l^2} \\[2mm] \dfrac{6EI}{l^2} & \dfrac{4EI}{l} & \dfrac{-6EL}{l^2} & \dfrac{2EI}{l} \\[2mm] \dfrac{-12EI}{l^3} & \dfrac{-6EI}{l^2} & \dfrac{12EL}{l^3} & \dfrac{-6EI}{l^2} \\[2mm] \dfrac{6EI}{l^2} & \dfrac{2EI}{l} & -\dfrac{6EL}{l^2} & \dfrac{4EI}{l} \end{bmatrix}$$
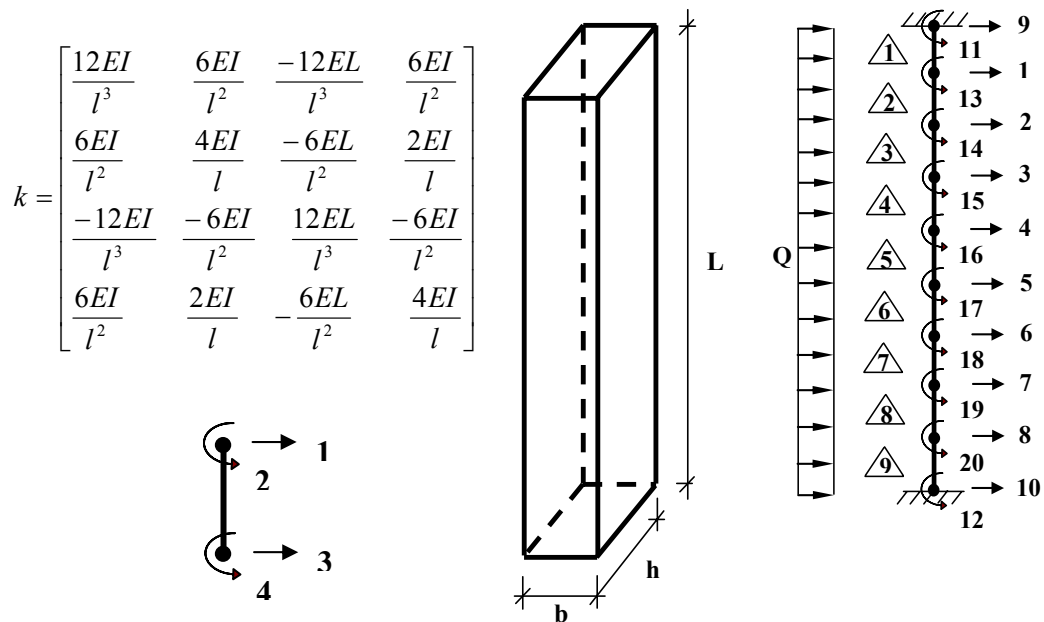
Figure 3.10 Description of analytical model

49

The static condensation method is used to eliminate from dynamic analysis those DOFs of the structure to which zero mass assigned. Typically the mass of the structure is idealized as concentrated in point lumps at nodes and the mass matrix contains zero diagonal elements in the rotational DOFs (Figure 3.10). These are the DOFs that can be eliminated from the dynamic analysis of the structure provided that the dynamic excitation does not include any external forces in the rotational DOFs [12].

If we write the equations motion for an MDF system subjected to external dynamic forces $p_j(t), j = 1 \ to \ N$. The dynamic response of the structure to this excitation is defined by the displacements $u_j(t)$, velocities $\dot{u}_j(t)$, and accelerations $\ddot{u}_j(t), \ j = 1 \ to \ N$.

$$m\ddot{u} + c\dot{u} + ku = p(t) \ [12] \tag{17}$$

$$\begin{bmatrix} m_{tt} & 0 \\ 0 & 0 \end{bmatrix} \begin{Bmatrix} \ddot{u}_t \\ \ddot{u}_o \end{Bmatrix} + \begin{bmatrix} k_{tt} & k_{t0} \\ k_{0t} & k_{00} \end{bmatrix} \begin{Bmatrix} u_t \\ u_0 \end{Bmatrix} = \begin{Bmatrix} p_t(t) \\ 0 \end{Bmatrix} \ [12] \tag{18}$$

Where u_0 denotes the DOFs with zero mass and u_t the DOFs with mass, also known as the dynamic DOFs; $k_{t0} = k_{0t}^T$. The two partitioned equations are

$$m_{tt}\ddot{u}_t + k_{tt}u_t + k_{t0}u_0 = p_t(t)$$

$$k_{0t}u_t + k_{00}u_0 = 0 \ [12] \tag{19}$$

$$u_0 = -k_{00}^{-1}k_{0t}u_t \ [12] \tag{20}$$

$$m_{tt}\ddot{u}_t + \hat{k}_{tt}u_t = p_t(t) \ [12] \tag{21}$$

Where $\hat{k}_{tt}$ is the condensed stiffness matrix given by

$$\hat{k}_{tt} = k_{tt} - k_{0t}^T k_{00}^{-1} k_{0t} \ [12] \tag{22}$$

Therefore,

$$k_{system} = \begin{bmatrix} k_{11_{(12x12)}} & k_{12_{(12x8)}} \\ k_{21_{(8x12)}} & k_{22_{(8x8)}} \end{bmatrix}_{20x20}$$

Boundary conditions are

δ_9, δ_{10}, δ_{11}, $\delta_{12} = 0$ and

$\delta_1,...,\delta_8$, $\theta_1,...,\theta_8 \neq 0$

Therefore,

$$\delta_{system} = \begin{bmatrix} \delta_{(8x1)} \\ 0 \\ 0 \\ 0 \\ 0 \end{bmatrix}_{(12x1)} \tag{23}$$

$$k_{system} \begin{bmatrix} \delta_{system} \\ \theta_{system} \end{bmatrix} = \begin{bmatrix} F \\ 0 \end{bmatrix} \tag{24}$$

$$k_{21}\delta_{system} + k_{22}\theta_{system} = 0 \tag{25}$$

$$k_{22}\theta_{system} = -k_{21}\delta_{system}$$

$$\theta_{system} = -k_{22}^{-1}k_{21}\delta_{system} \tag{26}$$

For each element,

$$\begin{bmatrix} V_1 \\ M_2 \\ V_3 \\ M_4 \end{bmatrix} = [k] \begin{bmatrix} \delta_1 \\ \theta_2 \\ \delta_3 \\ \theta_4 \end{bmatrix} \tag{27}$$

3.5.2 Construction of Classical Damping Matrix

The damping matrix is determined from modal damping ratios, which account for all energy-dissipating mechanism. Classical damping is an appropriate idealization if similar damping mechanisms are distributed throughout the structure [12]. Superposition of modal damping matrices is an alternative procedure of Rayleigh and Caughey to determine a classical damping matrix starting with equation (28).

$$\Phi^T c \Phi = C \tag{28}$$

Where C is a diagonal matrix with the *n*th diagonal element equal to the generalized modal damping with ζ_n estimated.

$$C_n = \zeta_n(2M_n\omega_n) \tag{29}$$

C is known from (28) and (29) can be written as

$$c = (\Phi^T)^{-1}C\Phi^{-1} \tag{30}$$

Starting with the orthogonality relationship,

$$\Phi^T m\Phi = M \tag{31}$$

It can be shown that

$$\Phi^{-1} = M^{-1}\Phi^T m \tag{32}$$

$$(\Phi^T)^{-1} = m\Phi M^{-1} \tag{33}$$

Substituting equation (33) in equation (31) leads to

$$c = (m\Phi M^{-1})C(M^{-1}\Phi^T m) \tag{34}$$

Can be expressed as

$$c = m(\sum_{n=1}^{N}\frac{2\zeta_n\omega_n}{M_n}\phi_n\phi_n^T)m \tag{35}$$

3.5.3 Stepwise Elastic Time History Analysis

If the applied force varies arbitrarily with the time, such problems can be tackled by numerical time stepping methods for integration of differential equations. For an inelastic system the equation of motion to be solved numerically is

$$m\ddot{u} + c\dot{u} + f_s(u,\dot{u}) = p(t) \text{ or } -m\ddot{u}_g(t) \text{ [12]} \tag{36}$$

Subject to the initial conditions

$$u_0 = u(0)$$

$$\dot{u} = \dot{u}(0)\,[12] \tag{37}$$

The applied force is given by $p_i = p(t_i)$, $i = 0$ *to* N. The time interval $\Delta t_i = t_{i+1} - t_i$ is taken to be constant.

The response is determined at the discrete time instants t_i, denoted as time I; the displacement, velocity, and acceleration are $u_i, \dot{u}_i$, and $\ddot{u}_i$, respectively. These values assumed to be known, satisfy equation (36) at time i:

$$m\ddot{u}_i + c\dot{u}_i + (f_s)_i = p_i \quad [12] \tag{38}$$

When applied successively with I=0, 1, 2, 3... the time-stepping procedure gives the desired response at all time instants I=1, 2, 3,... The known initial conditions, $u_0 = u(0)$ and $\dot{u}_0 = \dot{u}(0)$, provide the information necessary to start the procedure.

3.5.3.1 Central Difference Method

This method is based on a finite difference approximation of the time derivatives of displacement. Taking constant time steps, $\Delta t_i = \Delta t$, the central difference expressions for velocity and acceleration at time i are

$$\dot{u}_i = \frac{u_{i+1} - u_{i-1}}{2\Delta t} \tag{39}$$

$$\ddot{u}_i = \frac{u_{i+1} - 2u_i + u_{i-1}}{(\Delta t)^2} \quad [12] \tag{40}$$

Substituting these approximate expressions for velocity and acceleration into equation (38), gives

$$m\frac{u_{i+1} - 2u_i + u_{i-1}}{(\Delta t)^2} + c\frac{u_{i+1} - u_{i-1}}{2\Delta t} + ku_i = p_i \quad [12] \tag{41}$$

Transferring these known quantities to the right side leads to

$$\left[\frac{m}{(\Delta t)^2} + \frac{c}{2\Delta t}\right]u_{i+1} = p_i - \left[\frac{m}{(\Delta t)^2} - \frac{c}{2\Delta t}\right]u_{i-1} - \left[k - \frac{2m}{(\Delta t)^2}\right]u_i \quad [12] \tag{42}$$

or

$$\hat{k}u_{i+1} = \hat{p}_i \quad [12] \tag{43}$$

where

$$\hat{k} = \frac{m}{(\Delta t)^2} + \frac{c}{2\Delta t} \quad [12] \tag{44}$$

53

and

$$\hat{p}_i = p_i - \left[\frac{m}{(\Delta t)^2} - \frac{c}{2\Delta t} \right] u_{i-1} - \left[k - \frac{2m}{(\Delta t)^2} \right] u_i \quad [12] \tag{45}$$

The unknown u_{i+1} is then given by

$$u_{i+1} = \frac{\hat{p}_i}{\hat{k}} \quad [12] \tag{46}$$

The solution u_{i+1} at time $i+1$ is determined from the equilibrium condition, equation (38), at time i without using the equilibrium condition at time $i+1$. Such methods are called *explicit methods*.

$$\dot{u}_0 = \frac{u_1 - u_{-1}}{2\Delta t} \tag{47}$$

$$\ddot{u}_0 = \frac{u_1 - 2u_0 + u_{-1}}{(\Delta t)^2} \quad [12] \tag{48}$$

Solving for u_1 from the first equation and substituting in the second gives

$$u_{-1} = u_0 - \Delta t(\dot{u}_0) + \frac{(\Delta t)^2}{2} \ddot{u}_0 \quad [12] \tag{49}$$

Acceleration at time 0:

$$\ddot{u}_0 = \frac{p_0 - c\dot{u}_0 - ku_0}{m} \quad [12] \tag{50}$$

The central difference method will give meaningless results, in the presence of numerical round-off if the time step chosen is not short enough. The specific requirement for stability is

$$\frac{\Delta t}{T_n} < \frac{1}{\pi} \quad [12] \tag{51}$$

The central difference method derived so far was for the SDF systems. If the system has a few DOFs, it may be appropriate to solve these equations in their present form. Thus, the nodal displacements of the system are approximated by a linear combination of the first J natural modes:

$$u(t) \cong \sum_{n=1}^{J} \phi_n q_n(t) = \Phi q(t) \quad [12] \tag{52}$$

If we transform equation (38),

54

$$M\ddot{q} + C\dot{q} + Kq = P(t) \quad [12] \tag{53}$$

where

$$M = \Phi^T m \Phi \tag{54}$$

$$C = \Phi^T c \Phi \tag{55}$$

$$K = \Phi^T k \Phi \tag{56}$$

$$P(t) = \Phi^T p(t) \quad [12] \tag{57}$$

The central difference method can also be used for direct solution of the original equations in nodal displacements without transforming them to modal coordinates, by replacing q, $\dot{q}$, and $\ddot{q}$ by u, $\dot{u}$, and $\ddot{u}$; M, C, and K by m, c, and k; P by p; and K and $\hat{P}$ by $\hat{k}$ and $\hat{p}$.

3.5.4   Moment Curvature and Bilinearization Procedure

3.5.4.1   Material Models

3.5.4.1.1   Concrete Model Used In the M-K Analyses

In the analyses for generation of M-K relations of elements, the model for concrete under compression was selected as "Modified Kent and Park Model". According to this model, two distinct σ−ε models were proposed for confined and unconfined concrete. This model suggests an increase in strength and an elongation in the corresponding strain due to the confinement for confined concrete. Each σ−ε model combines a second order parabola for the initial branch and a first order function for the second branch. The σ−ε relations of concrete according to the "Modified Kent and Park Model" is given in Figure 3.11.
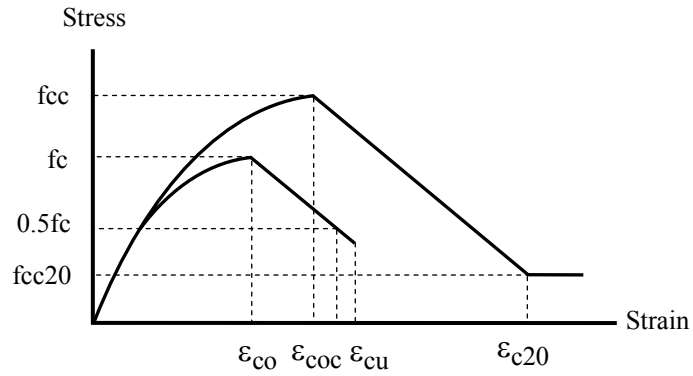
Figure 3.11 Modified Kent and Park Model

The functions of the parabola defined for unconfined concrete and confined concrete are given in Equations (58) and (59), respectively.

$$\sigma_c = f_c \left[\frac{2\varepsilon_c}{\varepsilon_{co}} - \left(\frac{\varepsilon_c}{\varepsilon_{co}} \right)^2 \right]$$

(58)

$$\sigma_c = f_c \left[\frac{2\varepsilon_c}{\varepsilon_{coc}} - \left(\frac{\varepsilon_c}{\varepsilon_{coc}} \right)^2 \right]$$

(59)

For the descending branch, the stress functions for unconfined and confined concrete are given in Equations (60) and (61), respectively.

$$\sigma_c = f_c \left[1 - Z_u (\varepsilon_c - \varepsilon_{co}) \right]$$

(60)

$$\sigma_c = f_{cc} \left[1 - Z_c (\varepsilon_c - \varepsilon_{coc}) \right] \geq 0.2 f_{cc}$$

(61)

where for unconfined concrete,

$$Z_u = \frac{0.5}{\varepsilon_{50u} - \varepsilon_{co}}$$

(62)

$$\varepsilon_{50u} = \frac{3 + 0.285 f_c}{142 f_c - 1000} \geq \varepsilon_{co}$$

(63)

for confined concrete

$$K = 1 + \frac{\rho_s \times fywk}{fc} \tag{64}$$

$$Z_c = \frac{0.5}{\varepsilon_{50u} + \varepsilon_{50h} - \varepsilon_{coc}} \tag{65}$$

$$\varepsilon_{50h} = 0.75 \rho_s \left(\frac{b_k}{s} \right)^{1/2} \tag{66}$$

$$\rho_s = \frac{A_0 \times l_s}{s \times b_k \times h_k} \tag{67}$$

$$f_{cc} = K \times f_c \tag{68}$$

$$\varepsilon_{coc} = K \times \varepsilon_{co} \tag{69}$$

In the program, ε_{c0} is taken as 0.002.

3.5.4.1.2   Steel Model

The model used for reinforcing steel is "Bilinear Model". In this model, the modulus of elasticity of the steel is used until the yielding of the steel. After yielding, the slope of post-yield branch defines the hardening characteristics of the steel model. Hardening stiffness is taken as % 5 of the initial stiffness of steel. The rupture of reinforcing steel (ε_{su}) is taken as 0.1 in the moment-curvature program. The material model of steel is given in Figure 3.12.
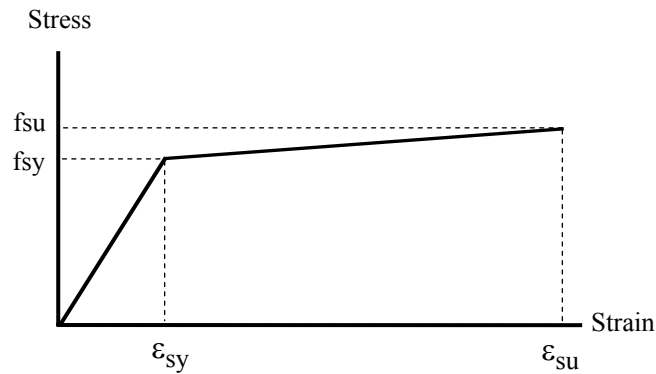
Figure 3.12 Steel Model

3.5.4.2 M - K Procedure

The moment - curvature diagram of a column element is obtained by utilizing a personal computer code which uses the material models explained in the previous section. In this code, after defining the key parameters, the material models are generated following the main rules. The section is divided into infinitesimal fibers for the stress and force calculations. For each value of outer concrete fiber strain and an assumed neutral axis position, the stress at each level and corresponding axial force is computed using the generated material models. Summing up the forces and taking moments about the neutral axis of the section, the net axial force and moment at this section is calculated.

Checking the axial force computed from these calculations with the net force on the column element, the necessity for doing iterations can be determined. If the difference between the axial force values is not in acceptable margins, a new neutral axis position has to be assumed and the calculations have to be repeated until obtaining real M-K value. For several M-K pairs, the calculations are repeated and at last the moment-curvature of the column element under a specified level of axial loading can be obtained.

3.5.4.3   Bilinearization

In order to be able to use the derived M-K relation of the structural element in the structural analyses and to simplify the calculations, the M-K relation obtained should be represented by simpler models, i.e. "Bilinear Model". To bilinearize the model, following rules are followed:

- The elastic portion of the bilinear model is determined using the initial branch of the original M-K relation
- The area under the bilinear model is tried to be kept same with the area under the original curve

- The yield point of the bilinear model is forced to be equal or less than the ultimate moment value of the original curve.

Using these simple rules, the original M-K curve is simplified to a bilinear M-K model.

3.5.5 Shear Strength of Concrete Section

Shear capacity of column is calculated according to ACI 318 as it is used in Turkish building code TS500. The shear strength is based on an average shear stress on the full effective cross section $b_w d$. In a member with shear reinforcement, a portion of the shear strength is assumed to be provided by the concrete and the remainder by the shear reinforcement.

$$V_n = V_s + V_c \tag{70}$$

V_s is nominal shear strength provided by shear reinforcement

V_c is nominal shear strength provided by concrete

Shear strength provided by shear reinforcement,

$$V_s = \frac{2A_s}{s} f_{yk} d \tag{71}$$

For members subjected to axial compression, shear strength provided by concrete,

$$V_c = 0.65 f_{ctd} b_w d \left(1 + 0.07 \frac{N_d}{A_c}\right) \tag{72}$$

Equ1 can be expressed as,

$$V_n = \frac{2A_s}{s} f_{yk} d + 0.65 f_{ctd} b_w d \left(1 + 0.07 \frac{N_d}{A_c}\right) \tag{73}$$

3.5.6 Strain Rate Effect

In order to investigate reinforced concrete elements under blast loading conditions, strain rate effect must be considered. Blast loads typically produce

very high strain rates in the range of $10^2 - 10^4$ s^{-1}. This high straining (loading) rate would alter the dynamic mechanical properties of target structures and, accordingly, the expected damage mechanisms for various structural elements. For reinforced concrete structures subjected to blast effects the strength of concrete and steel reinforcing bars can increase significantly due to strain rate effects. Figure 3.13 shows the approximate ranges of the expected strain rates for different loading conditions. It can be seen that ordinary static strain rate is located in the range: 10^{-6}-10^{-5} s-1, while blast pressures normally yield loads associated with strain rates in the range: 10^2-10^4 s^{-1} [1].
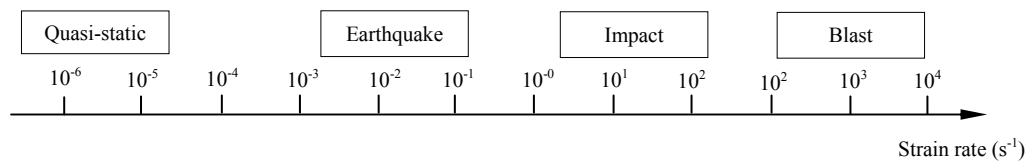
Figure 3.13 Strain rates associated with different types of loading [1]

Over the past century a large number of experiments have been carried out on the behavior of concrete prismatic or cylindrical specimens under high rates of uniaxial compressive loading. This difference primarily takes the form of an increase in the specimens' load-carrying capacity and maximum sustained axial strain, a difference which becomes more apparent as the loading rate increases. In order for such material models to be used in problems involving the investigation of structural concrete under static or dynamic loading, one must initially calibrate them carefully (based on the available experimental data) by assigning certain values to a number of parameters which are essential in order to fully define the material model. However, the use of such parameters usually makes the FE packages which incorporate them case-sensitive owing to the fact that their ability to produce accurate predictions is limited only to certain problem types. On the other hand, Cotsovos &

Pavlovic's work follows opposite approach: it employs the FE model to reproduce the experimental data and, in so doing, also aims to provide a fundamental explanation for the sudden increase in concrete strength and the overall change in the specimen behavior as a limiting value of loading rate is exceeded. The work is based on a nonlinear FE program, which incorporates a three-dimensional (3D) brittle material model of concrete behavior and has been shown to be capable of yielding realistic predictions of the response of a wide range of RC structures under static monotonically-increasing loads [15]. The results obtained from experiments investigating the behavior of prismatic and cylindrical concrete specimens under high rates of uniaxial compressive loading presented graphically in Figure 3.14.
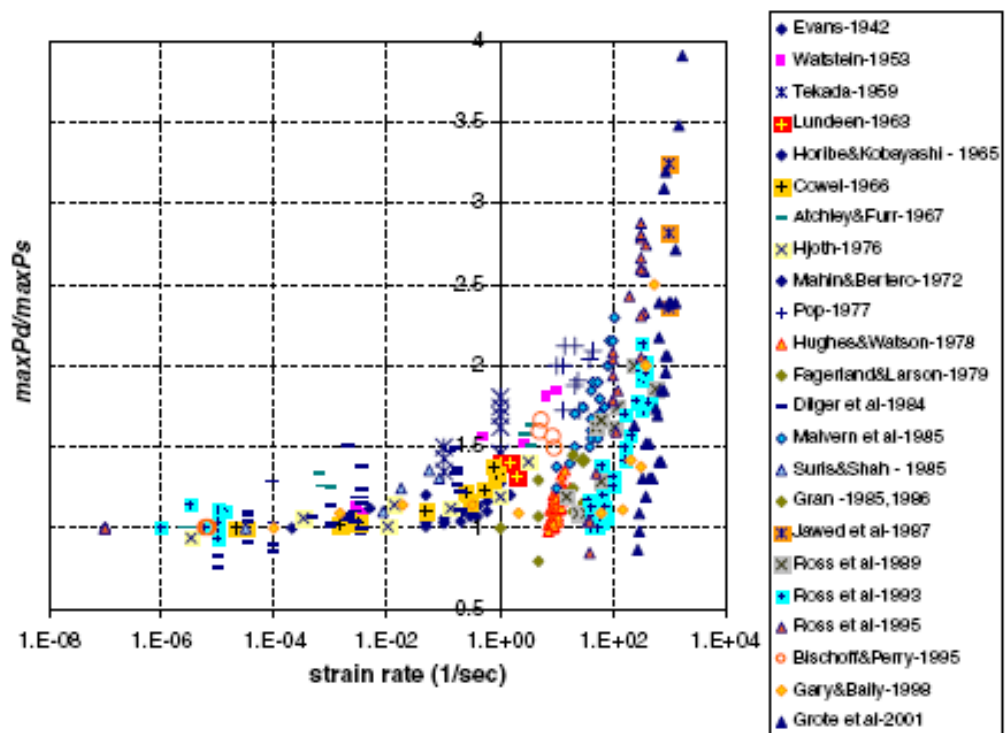
Figure 3.14 Variation of load-carrying capacity with strain rate for concrete in uniaxial compression [16]

Furthermore, when reviewing the details of the various experimental investigations carried out to date, it is apparent that a number of parameters (such as the static uniaxial compressive strength of concrete f_c, the experimental techniques used for the tests, the shape and size of the specimens, the density and moisture content of concrete, etc.) vary from one experiment to another [16]. In second part of Cotsovos & Pavlovic's investigation, these factors are considered as well as the combined effect of various factors which is included in this thesis. The maximum value of the average strain rate versus dynamic increase factor (DIF=P_d/P_s) is shown in Figure 3.15 and Figure 3.16.
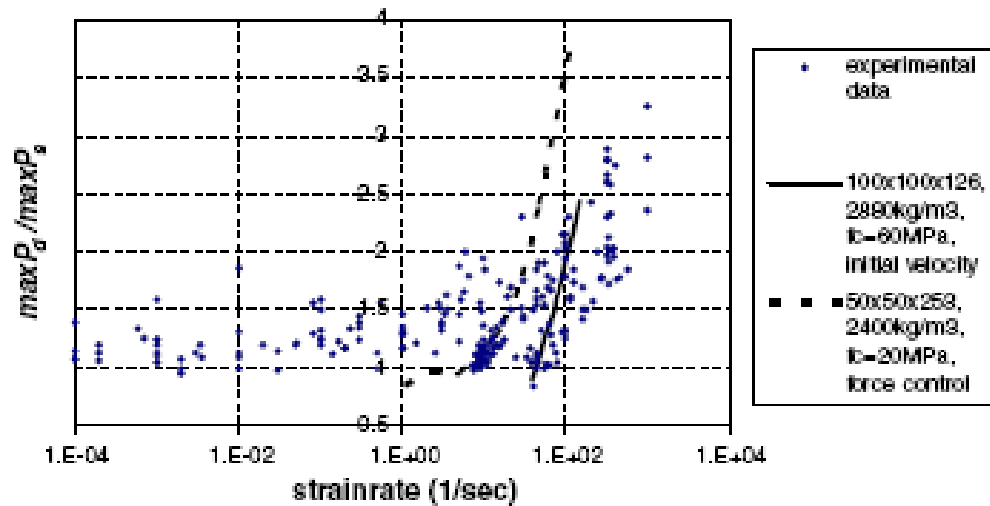
Figure 3.15 Numerical predictions for the extent of experimental scatter: variations of maxP$_d$/maxP$_s$ with maximum value of average strain rate and comparison with experimental data [16]
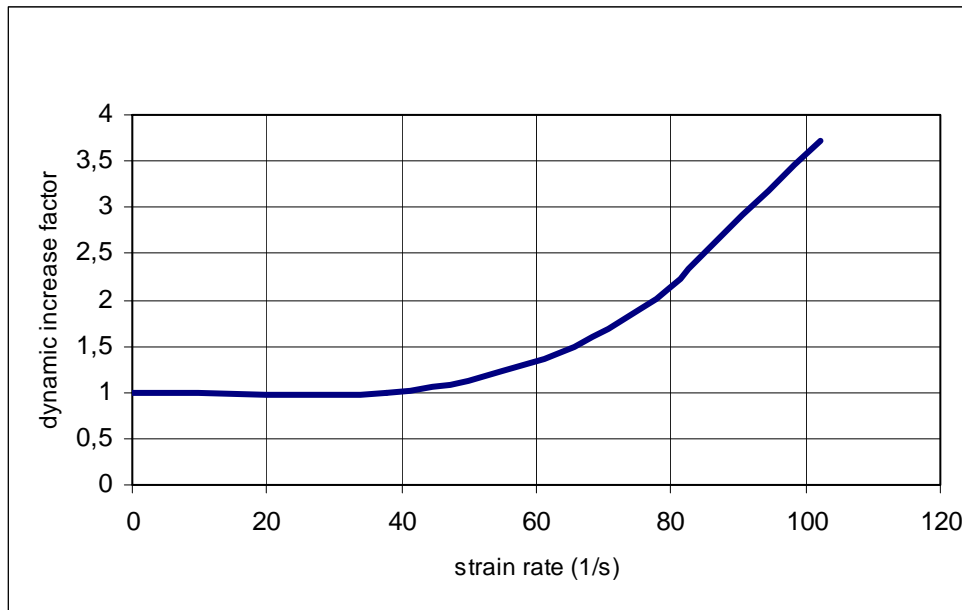
Figure 3.16 Dynamic increase factor vs. strain rate (redrawn from Figure 3.15-50x50x253 fc=20MPa force control)

3.6 SAMPLE PROBLEMS

The sectional analysis program of a column under blast load enables us to test for different cases and examine the results. By using the results, useful and simplified charts can be developed and used instead of working out calculations for every condition. In order to do this, columns designed as a part of ordinary structures are sampled and studied. Thus the results in parallel with the actual behavior can be produced.

Firstly 3 different sections were chosen (Figure 3.17). And the amount and the layout of the reinforcement in the section was defined by conjecturing that,

$$\frac{N}{A_c} \leq 0.3 f_{ck} \tag{74}$$

The columns were analyzed by shuffling the parameters which are distance to target (R_g), dimensions of column (b_w x h), effective charge weight (W) and

63

height of column (L). Materials are C20 for concrete and S420 for reinforcement.

| | 12Φ20 | 8Φ20 | 8Φ16 |
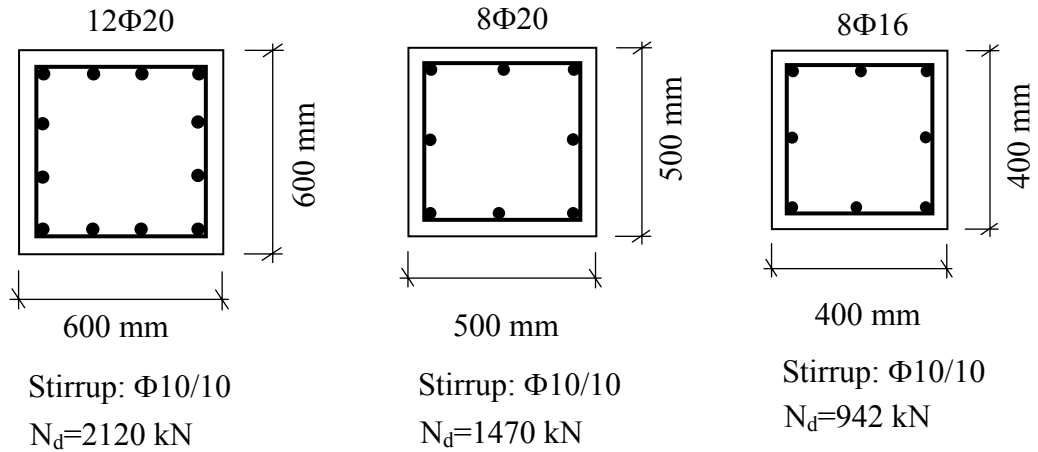
Figure 3.17 Sample sections

3.6.1 Demand-Capacity Relationship for Sections subjected to Blast Load

Bilinearized moment curvature diagrams are plotted for each sample sections. From the moment curvature curves theoretical moment capacities are obtained, which are the moment values at the end of the elastic range. Theoretical shear capacities of the sections are obtained in accordance with ACI 318-02 as described in chapter 3.5.5 of this thesis. These moment and shear capacities of the sections are increased according to strain rate effect and compared with the moment and shear values which are obtained through time stepping analysis, in which time step is taken to be 0.00001 sec. The height of the column is taken to be 3.5 m.
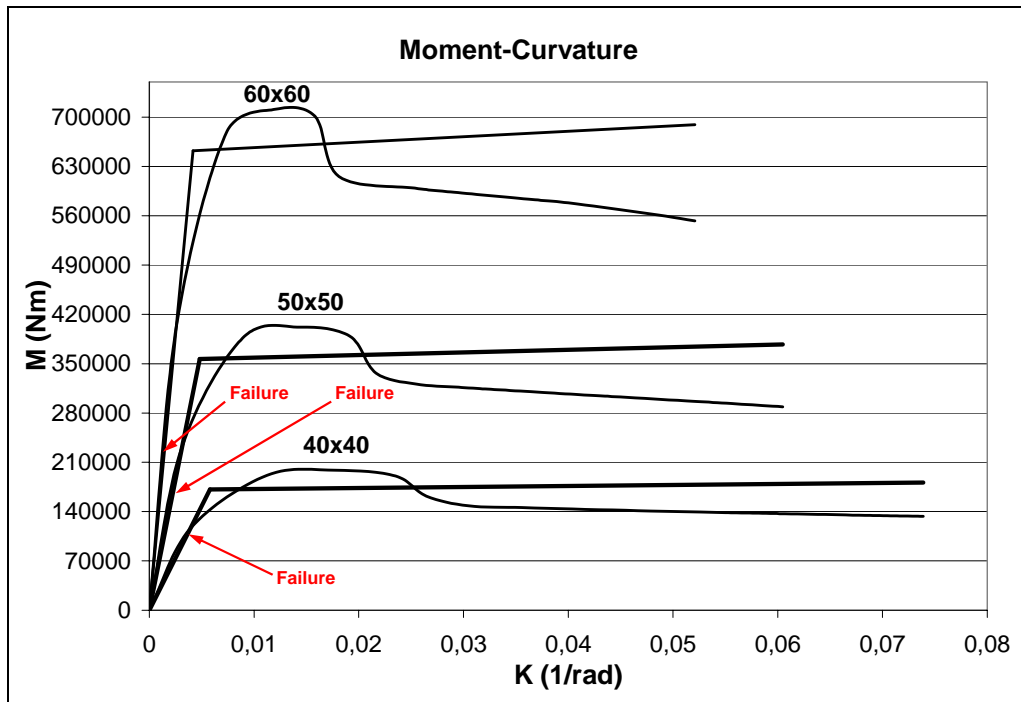
Figure 3.18 Moment-curvature diagrams of chosen sections
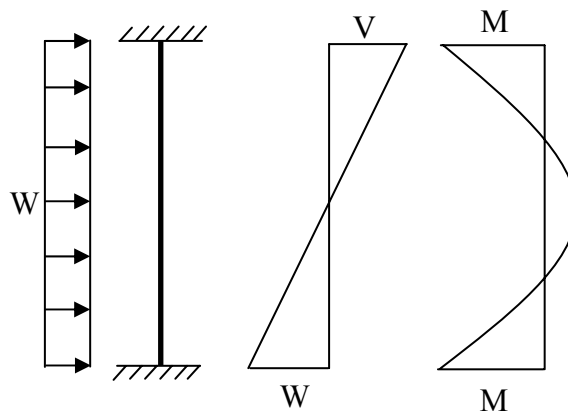
Figure 3.19 Typical shear and moment diagrams

$$M_{static} = \frac{WL^2}{12} \qquad\qquad (75)$$

$$V_{static} = \frac{WL}{2} \qquad\qquad (76)$$

At all steps, it is observed that initially the shear values reach to the capacity. Therefore, the sections failed due to the shear failure. Because moment demand-capacity ratios of column at time of shear failure are less than one (Table 3.1 column of I). Therefore shear failure occurs before column reaches its moment capacity. It will not be proper to make static calculations using peak pressures, since the peak pressures are instant and dynamic. Besides, dynamic movement of the column continues even after the loading is over. It can also be seen from the Table 3.1 (columns of J, K) that, dynamic shear and moment demands are much bigger than the capacities of the column. While the section dimensions of the columns increases, the time of shear failure decreases. Therefore increasing the rigidity of column causes early brittle shear failure at column.

3.6.1.1 P-Δ Effect

Bending moments affect columns in addition to axial load. Displacements from bending cause secondary effects together with axial load. This second-order behavior has been termed the P-Delta effect since the additional overturning moments on the column are equal to the sum of story weights (axial load) "P" times the lateral displacements "Delta". P-Delta effect can be calculated as it is seen in Figure 3.20. Displacements of middle height of column are obtained from the program and presented in Table 3.1 (column of L). Secondary moments are calculated as it is seen in Table 3.1 (column of N). These secondary moments are small when they are compared to moment from blast loading (Table 3.1 column of O). In other words P-Delta effect is not dominant in R/C columns when blast loading is considered.

66

Table 3.1 Output of Analysis

A	B	C	D	E	F	G	H	I	J	K	L	M	N	O
				CAPACITY					DEMAND			P-Δ EFFECT		
distance to target "R$_g$" (m)	dimensions of column "b$_w$ x h"	effective charge weight "W" (kg)	peak incident pressure "P$_a$" (kN/m)	shear capacity (kN)	moment capacity (kNm)	time of shear failure (msec)	moment at time of shear failure (kNm)	$\frac{moment\ demand}{moment\ capacity}$ ratio at time of shear failure	max. shear (kN)	max. moment (kNm)	max. disp. "Δ" (m)	axial load "P" (kN)	PxΔ (kNm)	max. moment + PxΔ (kNm)
5	40x40	2000	6524	374	171	5,51	92	0,54	5298	4008	0,0576	742	42,7058	4051
		1500	5925			5,65	91	0,53	4347	3265	0,0466		34,5557	3299
		1000	4928			6,10	92	0,54	3140	2326	0,0328		24,3331	2350
		750	4157			6,68	93	0,54	2408	1768	0,0247		18,3556	1786
		500	2934			8,29	94	0,55	1512	1101	0,0153		11,3333	1112
		400	2173			10,13	95	0,56	1102	801	0,0111		8,24065	809
		300	1812			11,05	97	0,57	909	660	0,0091		6,78618	667
		200	1244			13,94	106	0,62	694	508	0,0071		5,25982	513
5	50x50	2000	6524	524	357	5,32	129	0,36	8024	5990	0,0342	1470	25,3452	6015
		1500	5925			5,46	129	0,36	6442	4870	0,028		20,7389	4891
		1000	4928			5,88	129	0,36	4605	3479	0,0199		14,768	3494
		750	4157			6,44	130	0,37	3526	2650	0,0151		11,199	2661
		500	2934			8,00	132	0,37	2215	1655	0,0094		6,94705	1662
		400	2173			9,80	135	0,38	1615	1205	0,0068		5,05398	1210
		300	1812			10,70	140	0,39	1330	995	0,0056		4,16351	999
		200	1244			13,63	157	0,44	1015	762	0,0043		3,21464	765
5	60x60	2000	6524	695	652	5,20	172	0,26	1116	8200	0,0219	2120	16,2661	8216
		1500	5925			5,33	172	0,26	9080	6750	0,0182		13,4829	6763
		1000	4928			5,74	172	0,26	6350	4810	0,0131		9,73281	4820
		750	4157			6,29	175	0,27	4840	3670	0,01		7,42965	3677
		500	2934			7,82	178	0,27	3030	2290	0,0062		4,63565	2295
		400	2173			9,59	182	0,28	2210	1670	0,0045		3,37476	1673
		300	1812			10,48	189	0,29	1820	1380	0,0037		2,78131	1383
		200	1244			13,53	223	0,34	1393	1055	0,0029		2,13703	1057
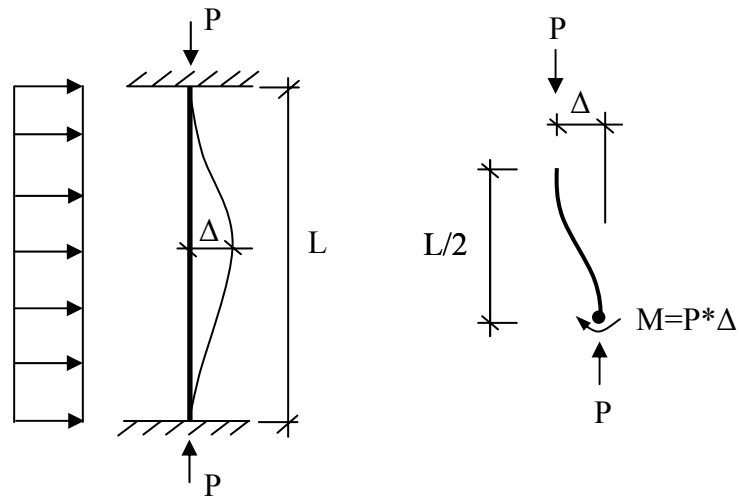
Figure 3.20 P-Delta effect of column

3.6.2 Analysis of Maximum Displacements

Without questioning the capacity of the element, maximum displacements are investigated.
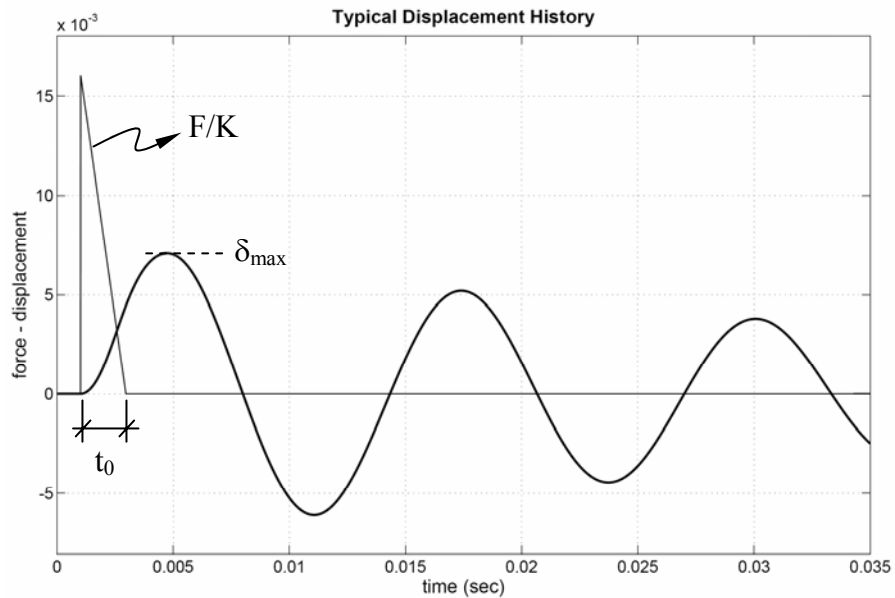
Figure 3.21 Typical displacement history

68

Table 3.2 Output of the analysis (40x40 column)

distance to target "R_g" (m)	dimensions of column "b_w x h"	effective charge weight "W" (kg)	height of column "L" (m)	peak incident pressure "P_a" (N/m)	total possitive impulse "t_0" (sec)	period "T" (sec)	maximum displacement at mid point of column "δ_{max}" (m)
5	40x40	2000	3	6524229	0,00315	0,00921	0,039
			3,5	6524229	0,00315	0,01254	0,058
			4	6524229	0,00315	0,01637	0,078
		1500	3	5924571	0,00276	0,00921	0,032
			3,5	5924571	0,00276	0,01254	0,047
			4	5924571	0,00276	0,01637	0,063
		1000	3	4927629	0,00231	0,00921	0,023
			3,5	4927629	0,00231	0,01254	0,033
			4	4927629	0,00231	0,01637	0,044
		750	3	4156714	0,00205	0,00921	0,017
			3,5	4156714	0,00205	0,01254	0,025
			4	4156714	0,00205	0,01637	0,033
		500	3	2934000	0,00177	0,00921	0,011
			3,5	2934000	0,00177	0,01254	0,015
			4	2934000	0,00177	0,01637	0,020
		400	3	2173371	0,00175	0,00921	0,008
			3,5	2173371	0,00175	0,01254	0,011
			4	2173371	0,00175	0,01637	0,015
		300	3	1812060	0,00172	0,00921	0,006
			3,5	1812060	0,00172	0,01254	0,009
			4	1812060	0,00172	0,01637	0,012
		200	3	1244289	0,00196	0,00921	0,005
			3,5	1244289	0,00196	0,01254	0,007
			4	1244289	0,00196	0,01637	0,009

Table 3.3 Output of the analysis (50x50 column)

distance to target "R_g" (m)	dimensions of column "b_w x h"	effective charge weight "W" (kg)	height of column "L" (m)	peak incident pressure "P_a" (N/m)	total possitive impulse "t_0" (sec)	period "T" (sec)	maximum displacement at mid point of column "δ_{max}" (m)
5	50x50	2000	3	6524229	0,00315	0,00737	0,022
			3,5	6524229	0,00315	0,01003	0,034
			4	6524229	0,00315	0,01310	0,048
		1500	3	5924571	0,00276	0,00737	0,018
			3,5	5924571	0,00276	0,01003	0,028
			4	5924571	0,00276	0,01310	0,039
		1000	3	4927629	0,00231	0,00737	0,013
			3,5	4927629	0,00231	0,01003	0,020
			4	4927629	0,00231	0,01310	0,027
		750	3	4156714	0,00205	0,00737	0,010
			3,5	4156714	0,00205	0,01003	0,015
			4	4156714	0,00205	0,01310	0,020
		500	3	2934000	0,00177	0,00737	0,006
			3,5	2934000	0,00177	0,01003	0,009
			4	2934000	0,00177	0,01310	0,013
		400	3	2173371	0,00175	0,00737	0,005
			3,5	2173371	0,00175	0,01003	0,007
			4	2173371	0,00175	0,01310	0,009
		300	3	1812060	0,00172	0,00737	0,004
			3,5	1812060	0,00172	0,01003	0,006
			4	1812060	0,00172	0,01310	0,008
		200	3	1244289	0,00196	0,00737	0,003
			3,5	1244289	0,00196	0,01003	0,004
			4	1244289	0,00196	0,01310	0,006

Table 3.4 Output of the analysis (60x60 column)

distance to target "R_g" (m)	dimensions of column "b_w x h"	effective charge weight "W" (kg)	height of column "L" (m)	peak incident pressure "P_a" (N/m)	total possitive impulse "t_0" (sec)	period "T" (sec)	maximum displacement at mid point of column "δ_{max}" (m)
5	60x60	2000	3	6524229	0,00315	0,00614	0,014
			3,5	6524229	0,00315	0,00836	0,022
			4	6524229	0,00315	0,01092	0,032
		1500	3	5924571	0,00276	0,00614	0,012
			3,5	5924571	0,00276	0,00836	0,018
			4	5924571	0,00276	0,01092	0,026
		1000	3	4927629	0,00231	0,00614	0,009
			3,5	4927629	0,00231	0,00836	0,013
			4	4927629	0,00231	0,01092	0,018
		750	3	4156714	0,00205	0,00614	0,007
			3,5	4156714	0,00205	0,00836	0,010
			4	4156714	0,00205	0,01092	0,014
		500	3	2934000	0,00177	0,00614	0,004
			3,5	2934000	0,00177	0,00836	0,006
			4	2934000	0,00177	0,01092	0,009
		400	3	2173371	0,00175	0,00614	0,003
			3,5	2173371	0,00175	0,00836	0,005
			4	2173371	0,00175	0,01092	0,006
		300	3	1812060	0,00172	0,00614	0,003
			3,5	1812060	0,00172	0,00836	0,004
			4	1812060	0,00172	0,01092	0,005
		200	3	1244289	0,00196	0,00614	0,002
			3,5	1244289	0,00196	0,00836	0,003
			4	1244289	0,00196	0,01092	0,004

Typical displacement history is examined at the midpoint of the column and the related graph is shown in Figure 3.21.

Maximum displacement of the column depends on geometry, magnitude of the load and the reinforcement provided inside.

Investigating an element under blast load requires including a number of parameters in the calculations. The outcomes, which are obtained by using the developed software (Table 3.2, Table 3.3, Table 3.4), are thoroughly investigated and some practical equations are derived.

3.7 EMPIRICAL RELATIONSHIPS

Recent studies reveal that, experimental outcomes about the blast load are in good agreement with the analytical results. Therefore throughout this thesis, blast load is calculated in accordance with the methods defined in the current specifications. These methods include calculation of parameters defined in Figure 2.14. Steps to find the parameters are:

$$\frac{H_c}{w^{1/3}} \quad \text{(scaled height of burst)}$$

$$a = \tan^{-1}\left(\frac{R_G}{H_c}\right) \quad \text{(angle of incidence)}$$

- Determine peak reflected pressure P_{ra} from Figure 2.14
- Determine scaled time of arrival of blast wave $\dfrac{t_A}{w^{1/3}}$
- Read scaled distance Z from Figure 2.14 for $P_{so} = P_{ra}$
- Determine scaled duration of positive phase from Figure 2.14 for the value Z

An Excel Sheet is prepared, using the steps defined above. A 3D graph is obtained assuming $H_c = 2.5$m to simplify the blast load calculation. A more useful chart, in which calculated pressure is in (N/m^2), is practically obtained using R_G (actual ground distance) and W (equivalent TNT charge weight). As can be seen in Figure 3.22, as the distance and weight of the explosion decreases, the effect of the explosion also decreases.
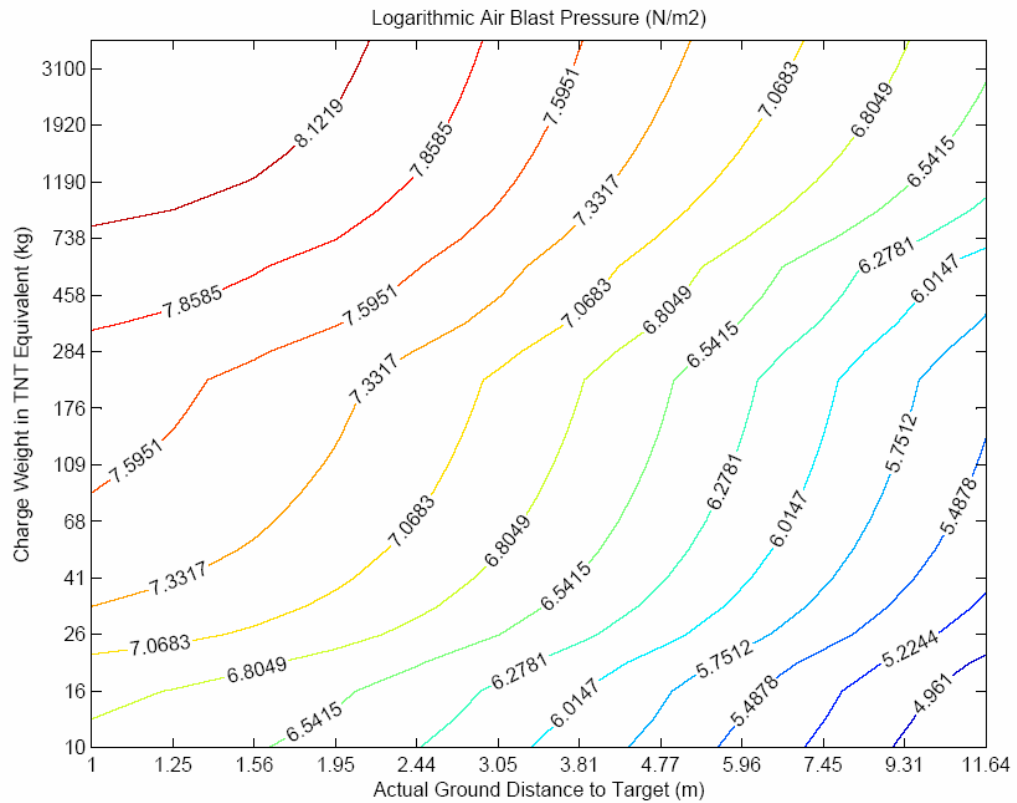
Figure 3.22 Air blast pressure

In this calculation method, the peak incident blast pressures in mach wave acting on ground surface are taken into account. Consequently, due to the reflected wave pressure, increase in the effect of the explosion can be observed in the results.

The program assumes the column as a single degree of freedom system under uniformly distributed load (Figure 3.23). Moving mass is half of the length of the column $\left(\dfrac{L}{2}\right)$ at the middle portion.
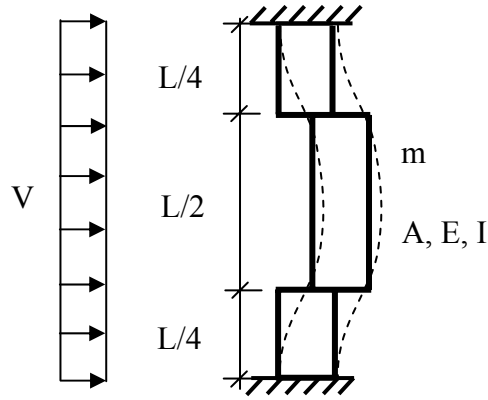
Figure 3.23 Typical SDF system of column

Accordingly, the stiffness of the column is

$$K = 2 \times \frac{12EI}{(L/2)^3} = \frac{192EI}{L^3} \tag{77}$$

The moving mass is

$$m = A \times \gamma_{concrete} \times \frac{L}{2} = A \times 2500t/m^3 \times \frac{L}{2} \tag{78}$$

And the period is

$$T = B \times \left(2\pi \sqrt{\frac{m}{K}} \right) \tag{79}$$

This calculated period is compared with the program output period which is also more realistic and calibrated with a coefficient B.

$$B = 1.1612 \tag{79}$$

$$T = 1.1612 \left(2\pi \sqrt{\frac{m}{K}} \right) \tag{80}$$

Maximum displacement of a column under a static load is

$$\delta_{max(static)} \approx \frac{WL^4}{384EI} \tag{81}$$

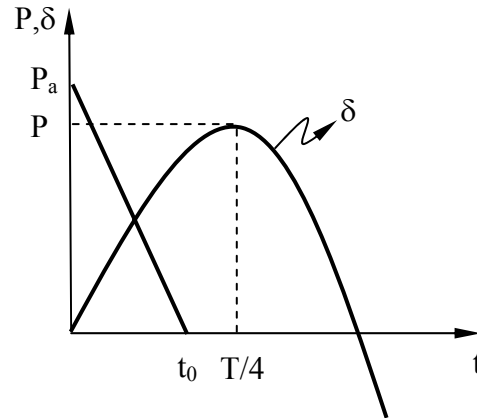$$W \approx Pb_w \text{ (uniformly distributed load)} \tag{82}$$

Figure 3.24 Pressure-time history

P is the calibrated pressure of the maximum incident pressure P_a, and represents the static loading at time $\left(\frac{T}{4}\right)$ (Figure 3.24). In order to be able to use P pressure in a wide variety of situations, P is shifted with a coefficient and modified in accordance with the analysis results. In the end, the following equation is obtained.

$$P = \frac{P_a}{t_0}(t_0 - \frac{T}{4}) \tag{83}$$

$$P \rightarrow P_{av} = \frac{4.7185 \times P_a + \left(\frac{P_a}{t_0}(t_0 - \frac{T}{4})\right)}{1 + 4.7185} \tag{84}$$

$$\delta_{\max} = C \times P_{av} \times b_w \times \frac{L^4}{EI} \times \left(\frac{t_0}{T}\right)^{0.518} \tag{85}$$

$$C = 18.6 \times 10^{-5} \tag{86}$$

Maximum displacements obtained through equation (84) is compared with the output displacements of the program and the correlation is plotted as dotted lines on the graph for all the data as seen in Figure 3.25.
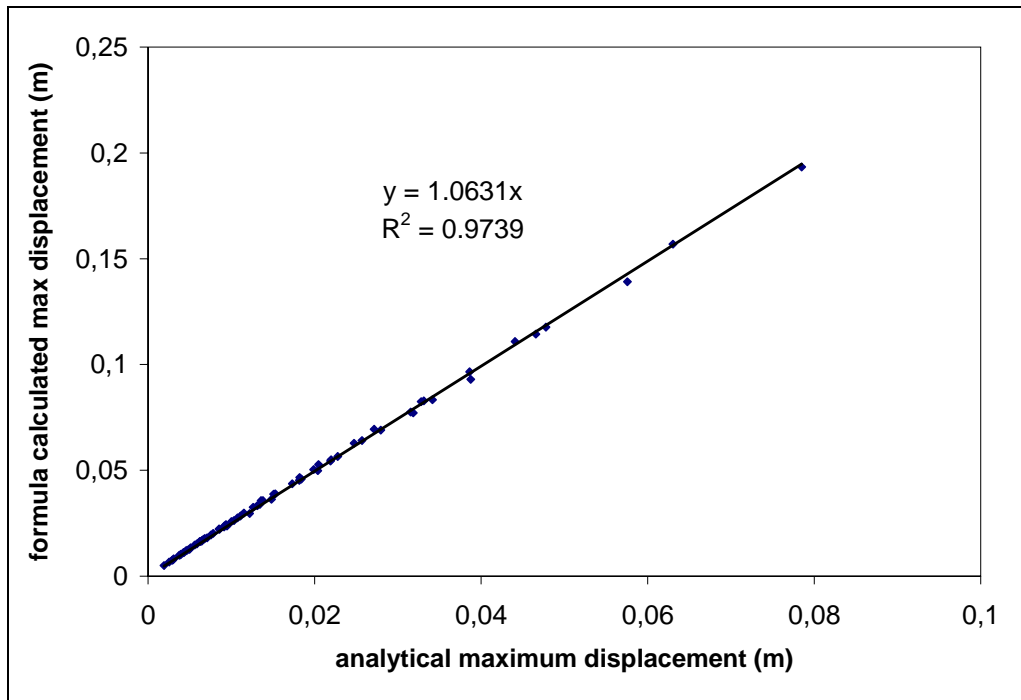
Figure 3.25 Best fit curve for obtained and calculated displacements

Equation (84) includes many parameters that effect the blast load. Therefore, it can be used to obtain reasonable solutions, without complicated calculations.

3.8 PRACTICAL METHODS

Analyzing the dynamic response of blast loaded structures has some complexities such as, strain rate effect, non-linear material behavior, time dependent deformations etc. Therefore a number of assumptions has been proposed to reach to a conclusion. Failure mode of a column subjected to blast load is generally shear failure. But sometimes if the length of a column is long enough, the failure mode becomes moment failure. It is important to know which failure mechanism would govern at the beginning of design or strengthening procedure. The moment failure is preferred in design calculations due to additional load capacity, ductility, and deformation capability. A sample

moment failure mechanism is shown in Figure 3.26. Distributed blast load, W_M, causes formation of three plastic hinge locations as the moments reach at the plastic moment capacity, M_p.
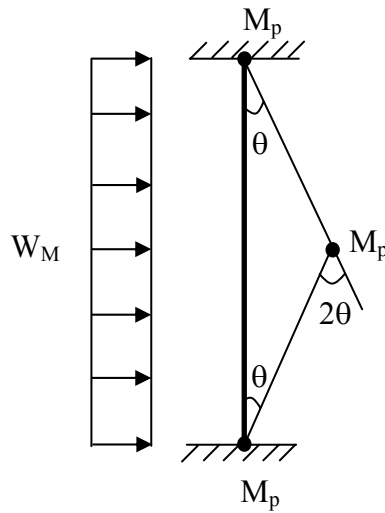
Figure 3.26 Plastic moments of a column

$$M_p \times 4\theta = W_M L \times (\frac{L}{2}\theta) \times \frac{1}{2} \tag{87}$$

$$M_{cap} = M_p = \frac{W_M L^2}{16} \tag{88}$$

$$W_M = \frac{16 M_{cap}}{L^2} \tag{89}$$

Figure 3.27 describes that distributed load, W_V causes each end joint of column reaches its shear capacity, V_{cap}.

Figure 3.27 Reactions and deform shape of a column

$$\frac{W_V L}{2} = V_{capacity} \tag{90}$$

$$W_V = \frac{2V_{cap}}{L} \tag{91}$$

If $W_M = W_V$ then

$$\frac{16M_{cap}}{L^2} = \frac{2V_{cap}}{L} \tag{92}$$

If $\dfrac{M_{cap}}{V_{cap}} < \dfrac{L}{8}$ then moment failure $\tag{93}$

If $\dfrac{M_{cap}}{V_{cap}} > \dfrac{L}{8}$ then shear failure $\tag{94}$

CHAPTER 4

CONCLUSIONS

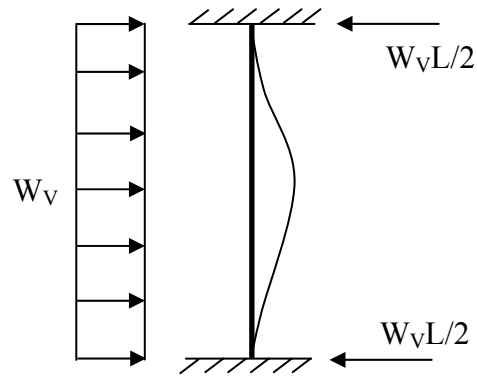## 4.1 CONCLUSIONS AND SUGGESTIONS

Blast loading characteristics and dynamic behavior of reinforced concrete columns subjected to blast loading are studied in this thesis. Matlab and Excel based computer programs to calculate load demand and capacity of R/C columns were developed. Comparison of static calculations and dynamic analysis results indicated that structural elements need to be analyzed dynamically since blast load changes as a function of time as well as application time is in terms of milliseconds. The blast load quickly diminishes as a function of distance and local members at the close proximity of the explosion are affected the most. Therefore, structural members' capacity and response at the location of the blast dictates the structural behavior different than the global parameters such as in the case of an earthquake. While loss of a beam would affect a single floor, loss of a column can be expected to affect all of the floors above the failing column. When a column is lost, the entire load transferred from the upper floors act on the beams which are probably partially damaged as well as weakened by doubled span length and missing tension reinforcement above the failed column. Partial collapse of all floors above a failed column is strongly expected in R/C buildings, although load redistribution takes place to some extend. Accuracy of this assumption can be investigated using linear of nonlinear progressive collapse analysis principles [28].

Examination of different column size blast loading analysis scenarios, it has been observed that failure is initiated by brittle shear failure at the supports rather than plastic hinge formations due to bending moment. Additionally P-delta effect is not considerable because it is small and R/C column fails until secondary moments are taken place. Consequently, any strengthening work increasing the shear capacity of the columns would also increase resistance against blast loading. Simple engineering calculations showed that increasing shear reinforcement in new buildings close to the joints would enhance the performance but may not be a solution for blast proof buildings. Wrapping columns to increase shear strength as well as bending moment capacity are frequently used in the literature. Converting the failure mechanism to moment failure from shear failure has advantages such as ductile behavior and larger deformation capacity. Wall-fence type of protection is also common to prevent approach of trucks or people with explosives near the important buildings.

Strain rates were calculated for each column and they were considered in calculations as a dynamic increase factor. Related to section 3.5.6, sudden increase in load carrying capacity of concrete was considered related to calculated strain rates. Uniformly distributed blast load was applied along the length of a column in this study. Bending was the dominant behaviour in this type of loading therefore maximum strain of column was expected to be smaller than the maximum strain of column which is subjected to uniaxial compressive loading. Thus the strain rates were in the range of 10^1-10^2 which is the impact loading region (Figure 3.13).

Simple design charts were developed to calculate the blast loading pressure on structural members as a function of explosive quantity (kg) and distance between the member and the explosion (m). Furthermore, empirical relationships were derived to calculate natural period of reinforced columns as well as maximum displacement demand under given loading condition and column dimensions.

This study showed the significance of blast loading evaluation in reinforced concrete buildings. The need to develop a special Turkish code for safety evaluation and design of blast load resistant buildings considering Turkish R/C building stock and design practice is necessary. It is suggested that a simple guideline should be developed, at least referring to some simple checks and empirical relationships to evaluate buildings under blast loading. American codes may not totally match the building practice and design codes in Turkey; therefore, customized guidelines should be developed.

The program and empirical equations developed in this thesis may be utilized to quickly check R/C columns and obtain an initial educated guess about the performance of structural columns when exposed to certain blast loading. If the members are found to be in the vicinity of blast critical condition, more detailed professional programs can be used to assess the exact response. The current software may be further improved to incorporate reduction in stiffness during loading and conduct a nonlinear analysis by modifying stiffness matrix at each loading level. However, a linear analysis is also expected to reveal if the column would pass its elastic limit or not. In the case of commonly available designs, the failure would be dominated by shear which is a brittle failure. The current program is expected to closely represent performance of R/C columns under blast loading.

4.2 FUTURE STUDIES

The following related subjects shall be further investigated,
- Modification of stiffness matrix for stiffness degradation to be added to the program.
- Comparison of analysis results with actual blast loading experiments or commercially available blast load analysis simulation results.
- Simulation of cover concrete loss.

82

- There are a number of unanswered questions regarding of other structural elements and entire structures. Load redistribution of a structure shortly after collapse of a column due to an explosion.
- Simulation of negative phase duration (suction effect) of blast loading

REFERENCES

[1]   Ngo T., Mendis P., Gupta A. & Ramsay J., *Blast Loading and Blast Effects on Structures*, EJSE Special Issue: Loading on Structures, 2007

[2]   Smith P.D., Hetherington J.G., *Blast and Ballistic Loading of Structures*, Butterworth-Heinemann Ltd., Great Britain, 1994

[3]   TM 5-1300, *The Design of Structures to Resist the Effects of Accidental Explosions*, Technical Manual, US Department of the Army, Navy, and Air Force, Washington DC, 1990

[4]   Osteraas J.D., *Murrah Building Bombing Revisited: Qualitative Assessment of Blast Damage and Collapse Patterns*, Journal of Performance of Constructed Facilities, ACSE, November 2006

[5]   Luccioni B.M., Ambrosini R.D., Danesi R.F., *Analysis of Building Collapse under Blast Loads*, Elsevier Ltd., 2003

[6]   http://www.okcbombing.org/images/1114.jpg, last accessed: 15.12.2007

[7]   http://www.thegully.com/essays/argentina/imgs-ar/bombed_AMIA_ar.jpg, last accessed: 04.02.2008

[8]   *User's Guide for the Single-Degree-of-Freedom Blast Effects Design Spreadsheets (SBEDS)*, U.S. Army Corps of Engineers Protective Design Center Technical Report, 2006

[9]   http://www.ara.com/products/ATblast.htm, last accessed: 04.02.2008

[10]   *Federal Emergency Management Agency, (FEMA) 427-Primer for Design of Commercial Buildings to Mitigate Terrorist Attacks*, December 2003

[11]   http://www.globalsecurity.org/military/intro/ied-vehicle.htm, last accessed: 04.02.2008

[12]   Chopra A.K., *Dynamics of Structures*, Prentice Hall, New Jersey, 2001

[13]   Lu B., Silva P.F., *Estimating Equivalent Viscous Damping Ratio for RC members under Seismic and Blast Loadings*, Elsevier Ltd., 2006

[14]   Ngo T.D., Mendis P.A., Teo D. & Kusuma G., *Behavior of High Strength Concrete Columns Subjected to Blast Loading*, University of Melbourne, Australia

[15]   Cotsovos D.M., Pavlovic P.M., *Numerical Investigation of Concrete Subjected to Compressive Impact Loading. Part 1: A Fundamental Explanation for The Apparent Strength Gain at High Loading Rates* Elsevier Ltd., 2007

[16]   Cotsovos D.M., Pavlovic P.M., *Numerical Investigation of Concrete Subjected to Compressive Impact Loading. Part 2: Parametric Investigation of Factors Affecting Behavior at High Loading Rates*, Elsevier Ltd., 2007

[17]   Dawe D.J., *Matrix and Finite Element Displacement Analysis of Structures*, The Oxford Engineering Science Series, Claredon Press, 1984

[18]   McGuire W., Gallagher R.H., Ziemian R.D., *Matrix Structural Analysis*, John Wiley & Sons, Inc., 2000

[19]   McCann D.M., Smith S.J., *Blast Resistant Design of Reinforced Concrete Structures*, Structure Magazine, April 2007

[20]   Crawford J.E., Malvar L.J., Morrill K.B., *Reinforced Concrete Column Retrofit Methods for Seismic and Blast Protection*

[21]   Ambrosini D., Luccioni B., Danesi R., *Influence of The Soil Properties on Craters Produced by Explosions on The Soil Surface*, Mecanica Computacional Vol. XXIII, Argentina, November 2004

[22]   *ACI 318-02 ACI 318R-02*, Building Code Requirements for Structural Concrete and Commentary, 2002

[23]   *Federal Emergency Management Agency*, (FEMA) 426-Referance Manual to Mitigate Potential Terrorist Attacks Against Buildings, December 2003

[24]   *Federal Emergency Management Agency*, (FEMA) 428-Primer for Designing Safe School Projects in Case of Terrorist, December 2003

[25]   Uzunoğlu M., Onar Ö.Ç., *Kolay Anlatımı ile İleri Düzeyde MATLAB 6.0-6.5*, Türkmen Kitabevi, 2002

[26] Ersoy U., *Reinforced Concrete*, Middle East Technical University, Ankara, 2000

[27] Prugh R.W., *The Effects of Explosive Blast on Structures and Personnel*, Process Safety Progress, Vol.18, No.1, 1999

[28] Tahmilci F, *Analysis of Blast Loading Effect on Regular Steel Building Structures*, METU, December 2007